California Energy Commission
Public Interest Energy Research Program

HPCBS # E4P23T1a & T2B

HPCBS

High Performance Commercial Building Systems

Documented models for EnergyPlus (4 Documents):

Defining a Global Room Surface Heat Transfer Coefficient
Room ventilation& heat transfer in unmixed spaces (PPT)
Contributions to Simplified Modeling of Building Airborne Pollutant Removal
Simplified Modeling of Cross-Ventialtion Airflow

Element 4. Low Energy Cooling
Project 2.3 - Tools and Guides

Carrilho da Graça, G. and Linden, P.F.
University Of California, San Diego

July, 2002

pier
"Research Powers the Future"

BERKELEY LAB

United States Department of Energy
Science, Security and Energy: Powering the 21st Century

Acknowledgement

This work was supported by the California Energy Commission, Public Interest Energy Research Program, under Contract No. 400-99-012 and by the Assistant Secretary for Energy Efficiency and Renewable Energy, Building Technologies Program of the U.S. Department of Energy under Contract No. DE-AC03-76SF00098.

DEFINING A GLOBAL ROOM SURFACE HEAT TRANSFER COEFFICIENT

Carrilho da Graça G., Linden P. F.. University of California at San Diego.
UCSD EBU II, 9500 Gilman Drive, La Jolla, CA 92093-0411. 858-8223184 gcg@ucsd.edu

Summary
This paper presents a simple conceptual approach to room surface convective heat transfer for two room ventilation strategies: mixing and cross-ventilation. A global room heat transfer coefficient is defined, clearly quantifying the reduction in heat transfer due to the finite heat capacity and recirculations that occur in the ventilation flow, allowing for direct analytical comparison with perfect mixing ventilation systems. The approach used in this study seeks to capture the dominant physical processes for these problems with first order precision and to develop simple analytical convective heat transfer models that show the correct system behavior trends.

Introduction
Cross-ventilation (C-V) occurs whenever the inflow air maintains a significant portion of its momentum flux as it travels across the room. In contrast, an ideal mixed ventilation system achieves complete diffusion of the inflow momentum. Mixing ventilation is common in most air-conditioned buildings while C-V is used in most wind driven ventilated buildings and in passive cooling systems relying on night cooling strategies (either naturally driven or hybrid).
The most commonly used room surface convective heat transfer models use a single modeling point to characterize ventilation air temperature. This approach is used in most building thermal simulation tools, in spite of the significant sensitivity of building energy consumption predictions to surface heat transfer coefficients. As will be shown below, single node models, or zero dimension models, are very imprecise in C-V heat transfer, failing to predict the magnitude of the heat transfer and translate most room geometry induced effects. This imprecision is a consequence of two approximations.
a) Room air is considered fully mixed: this approximation neglects the effects of the gradual temperature variations that occur as air moves across a room or in any other flow paths that can occur and that lead to contact with internal surfaces and heat sources. This results in inaccurate calculation of the overall thermal capacity of the airflow and in the inability to predict temperature variations inside the room. With this approximation, even if the correct local heat transfer coefficient is used the result can still be quite imprecise.
b) Incorrect local heat transfer coefficient: difficulties in determining the local heat transfer coefficient lead most modelers to use a constant averaged value, ignoring temperature and airflow pattern dependence.
As an alternative to this very simple modeling approach, computational fluid dynamics (CFD, solving the Reynolds averaged Navier Stokes equations in conjunction with the $k\varepsilon$ turbulence model) is gaining increased acceptance among designers. Due to the influence of the room surfaces in the airflow pattern, the use of CFD for ventilation heat transfer simulation requires detailed near wall models and careful monitoring of the results, often not feasible in building design situations.
Further, CFD, just like the one node approach fails in providing simple insight into the mechanisms and system parameters that control the heat transfer process. In this simplified modeling work we seek the correct determination of these parameters and their influence, while keeping first order precision. By introducing the concept of global room heat transfer coefficient h_G we will be able to show the effect of the ventilation flow pattern and the confinement effects caused by the presence of the room in the efficiency of the convective heat transfer process in mixing and C-V ventilation systems, extending the current zero dimension model to one and two dimensions (see cases C and R below).
Ventilation air can change temperature as it is exposed to different sub portions of the room surfaces. Figure 1 shows, schematically, the differences between flat plate heat transfer (the basic component of room heat transfer, see 1-a), and C-V. While flat plate heat transfer occurs at constant free stream temperature (T_{IN}=T_{OUT} in 1-a) any ventilation system will have variable temperature gradients as the air

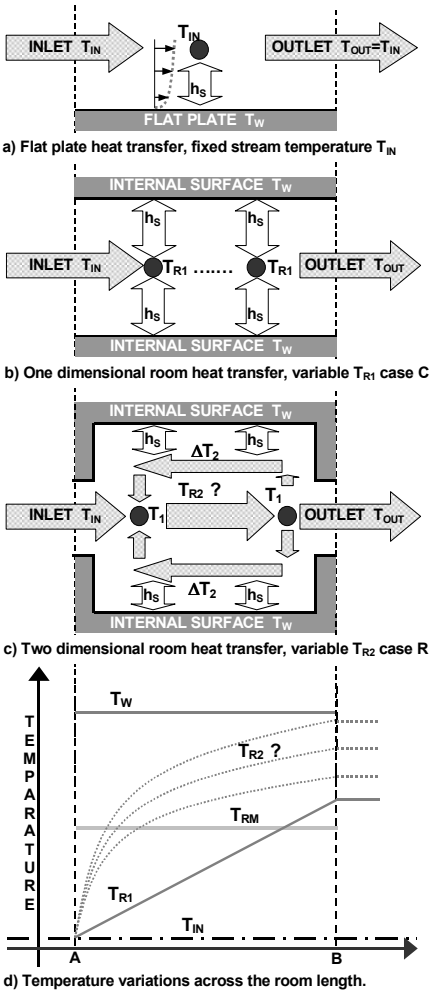

Figure 1.

a) flat plate heat transfer, fixed free stream temperature T_{IN}, and average surface heat transfer coefficient h_s
b) one dimensional room heat transfer.
c) two dimensional room heat transfer.
d) temperature variations for 1-a,b and c.

temperature changes along the flow pattern (see T_{R1} and T_{R2} in figures 1-b,c,d), as a consequence of heat transfer into a flow stream with limited heat capacity (determined by the finite ventilation flow rate). In a one node, fully mixed model the room temperature is constant (see T_{RM} in figure 1-d). The temperature gradients that determine the heat transfer with the room surfaces will be incorrectly modeled, whenever mixing is not perfect. Imperfect mixing happens in any room, in particular in C-V rooms or in rooms with displacement ventilation systems.

Due to the presence of a forced component (the ventilation flow) and a temperature difference, any heat transfer process in building ventilation occurs through mixed convection, as a result of forced (h_F) and a natural convection component (h_N). In order to predict the local mixed convection heat transfer coefficient that results from these two mechanisms, the following formula can be used (Seibers et al., 1983):

$$h_S = (h_F{}^{\varepsilon} + h_N{}^{\varepsilon})^{1/\varepsilon}, \qquad (1)$$

where ε, is a correlation constant, obtained from experiments. This formula has been used in two other studies that are relevant to the present work: with vertical surfaces in horizontal forced flow (Neiswanger et al., 1987) and horizontal surfaces with horizontal and vertically impinging forced flow (Awbi et al., 2000). In both studies, (1) was found to agree with experimental measurements when ε=3.2. Forced convection in turbulent boundary layer flow can be estimated using Colburn's analogy, establishing a direct relation between momentum and convective heat transfer:

$$St_x\, Pr^{2/3} = \tfrac{1}{2} C_{fx}, \qquad (2)$$

where C_{fx} is the skin friction coefficient and S_{tx} is the Stanton number. Using (1)and (2), in conjunction with the correlations proposed by Awbi et al., it is possible to conclude that natural convection dominates the mixed heat transfer process for typical room geometric parameters and flow rates whenever the characteristic near surface velocity is smaller than 0.2 m/s. This happens in most mixed and C-V systems, therefore, in the present analysis, we will only consider natural convection. In addition a unique heat transfer coefficient will be used for all room surfaces (considered to be at constant temperature T_S):

$$h_S \approx h_N,\ h_N \approx 1.6\,\Delta T^{1/3},\ \Delta T = (T_\infty - T_S)$$
$$q_w = h_S \Delta T = h_B\,\Delta T^{4/3},\ h_B = 1.6 \qquad (3)$$

$$q_{wA} = h_B(a.\Delta T - b),\ 1.5 < \Delta T < 5$$
$$a = 1.17,\ b = 0.725 \qquad (4)$$

The error introduced by both approximations in the ΔT interval shown is below 10% in most rooms, acceptable for this study.

Defining h_G in mixing ventilation

When designing for maximum surface heat transfer, the most relevant result is the total temperature change of the air (for a given flow rate). In order to simplify the analysis we will obtain a global room heat transfer coefficient h_G, as follows:

$$Q = h_G\, A_S\, (T_S - T_{IN}) \qquad (5)$$

where Q (W) is the total heat transfer between the compartment surfaces and the airflow, h_G ((W/(m^{2}K))) is the global heat transfer coefficient. A_S (m^2) is the total room surface

area, T_{IN} (K) is the average inlet airflow temperature and T_S (K) is the average internal surface temperature.
As a consequence of energy conservation Q equals the energy variation of the air flowing through the room (neglecting viscous heating):

$$Q = h_G A_S (T_S - T_{IN}) = \rho C_p F (T_{OUT} - T_{IN}) . \quad (6)$$

Here F (m^3/s) is the ventilation flow rate, ρ (Kg/m^3) is the air density, C_p (J/(Kg.K)) is the heat capacity of the air at constant pressure and T_{OUT} (K) is the average temperature of the air leaving the room.
In a mixed system $T_{OUT}=T_{RM}$, where T_{RM} is the mixed room air temperature, see figures 1b and d. In this case, introducing h_S to calculate the air to room surface heat transfer and using (5) and (6) leads to h_G for the full mixed, zero dimension case:

$$\begin{cases} h_S A_S (T_S - T_{RM}) = \rho C_p F (T_{RM} - T_{IN}) \\ h_G A_S (T_S - T_{IN}) = \rho C_p F (T_{RM} - T_{IN}) \end{cases} \Leftrightarrow \quad (7)$$

$$h_G = \frac{h_S}{\alpha + 1} , \alpha_S = \frac{h_S A_S}{\rho C_p F}, \alpha_B = \frac{h_B A_S}{\rho C_p F}$$

Further, introducing the linear approximation shown in (4) in the left hand side of the first equation in (7) leads to

$$h_G = \frac{(a - b/T_S - T_{IN}) h_B}{a.\alpha_B + 1}, \quad q_G = \frac{q_S}{a.\alpha_B + 1} \quad (8)$$

here q_G (W/m^2) is a heat flux per second, it is related to q_S in an similar way as h_G to h_S.
Although (8) depends on the temperature difference (T_S-T_{IN}) this dependence is simple. In both expressions, in the denominator, the fixed heat transfer coefficient (h_S) is replaced by the variable part of the approximated coefficient ($a.h_B$).
From simple analysis of (7) and (8), we see that h_G is proportional to the volumetric flow rate and, as expected, h_G<h_S. Note that h_S is, by definition, the heat transfer coefficient applicable when directly exposing the compartment surfaces to outside air, with no loss of heat transfer due to room confinement effects (case a in figure 1).
The fraction in the denominator is a non-dimensional system parameter that scales airflow rate heat capacity with surface heat transfer capacity, it could have been guessed by inspection and dimensional analysis principles. This formula quantifies the known fact that when all room parameters are fixed, the temperature change of the airflow is reduced when the flow rate increases. This reduced temperature change increases the average temperature difference between air and room surfaces, increasing heat transfer. When the heat transfer coefficient is dominated by natural convection this increase in h_G with the flow rate is higher, see (8).

Defining h_G in cross-ventilation

The two cross ventilation geometries that will be analyzed are shown in figures 1-b (case C, similar to flow in a corridor) and 1-c (case R when recirculations are present). Recirculating flow occurs whenever the inlet (often a window or a door) is much smaller than the room cross section, while case C occurs when inlet and cross section have similar magnitudes.

Case C

In this case, the ventilation flow changes its temperature along the path monotonically from inlet to outlet, clearly leading to a one dimensional model. There are no recirculation regions and the heat transfer process can be modeled using a single differential equation. The equation for the variation of the temperature along the x axis (in the C-V direction) for flow in a room with perimeter P and heated surfaces with temperature (T_S), using a fixed value for the heat transfer coefficient (h_S), is:

$$P = \frac{A_S}{L}; \ \rho C_p F \frac{\partial T(x)}{\partial x} = P h_S (T(x) - T_S) \Rightarrow \quad (9)$$

$$T(x) = T_S - e^{-\frac{h_S . P . x}{\rho . C_p . F}} (T_S - T_{IN})$$

where L (m) is the room length. When the temperature dependent heat transfer coefficient (see (3)) is used an analytical solution is also possible but is, as in the mixed case, cumbersome and dependent on the temperature difference in several terms making simple interpretation impossible. In order to simplify the result, (4) is used, resulting in the following temperature variation:

$$T(x) = (T_S - T_{IN} - \tfrac{b}{a})(1 - e^{F(x)}), F(x) = \tfrac{-a.h_B.P.x}{\rho.C_p.F} \quad (10)$$

and the value of $F(x)$ is small for typical rooms. As a consequence, it is possible to use a further approximation: linear temperature variation. In addition the heat transfer coefficient will be evaluated at the intermediate value of the temperature variation; h_G is then obtained by solving the following system of equations:

$$\begin{cases} \rho.C_p.F.\Delta T = A_S.h_B.(a.(T_S - T_{IN} - \frac{\Delta T}{2}) - b) \\ \rho.C_p.F.\Delta T = A_S.h_G.(T_S - T_{IN}) \end{cases} \Rightarrow$$

$$h_G = \left(a - \frac{b}{T_S - T_{IN}} \right) \frac{h_B}{a.\alpha_B \frac{1}{2} + 1} \quad (11)$$

The result is very similar to the fully mixed case (8), the difference is the factor of ½ that

multiplies the non-dimensional ratio in the denominator. As a consequence of this factor the one dimensional heat transfer coefficient is always higher than the fully mixed. It is more effective to exchange heat with the surfaces of a compartment in a case C flow configuration than in fully mixed mode.

Case R

Figure 1-c shows the locations of the points used in zoning the heat transfer model for this two dimensional case. Ventilation air enters the room with temperature T_{IN}. As the inlet jet entrains room air in the initial part of its propagation path, it changes its temperature to T_1 (the entrained air returns to the jet with a different temperatures since the room surfaces are at different temperature from the inlet air). In the second part of the path, the jet rejects the entrained air before it exits the room with temperature T_1. As the jet expels air, it feeds the recirculation flow that will exchange heat with the room surfaces and be re-entrained. In the recirculation, the air has a temperature change of ΔT_2 and returns to point T_1 where it merges with the inlet flow with temperature: $T_1+\Delta T_2$. The approximations used to analyze case C also apply to the recirculation flow. A correlation for maximum recirculation volumetric flow rate F_{RM} is used (Carrilho da Graca et al., 2002)

$$F_{RM} = 0.147\sqrt{{}^{L\,A_R}\!/\!_{A_{IN}{}^{3/2}}}\,F, \qquad (12)$$

where A_R is the room cross-section area and A_{IN} is the inlet area. Analyzing figure 1-c it is clear to see that T_1, ΔT_2, and h_G can be obtained by solving the following equations:

$$\rho.C_p.(F+F_{RM}).T_1 = \rho.C_p.(F.T_{IN}+F_{RM}.(T_{IN}+\Delta T_2))$$
$$\Delta T_2 = h_B.A_S.(a.(T_S - T_1 - \Delta T_2/2) - b).(\rho.C_p.F_{RM})^{-1}$$
$$A_S.h_G.(T_S - T_{IN}) = \rho.C_p.F.(T_1 - T_{IN}) \qquad (13)$$

and we obtain h_G:

$$h_G = \frac{\left(a - {}^{b}\!/\!_{T_S - T_{IN}}\right).h_B}{\frac{a.h_B.A_S}{\rho.C_p.F}\left(\frac{1}{0.147}\sqrt{{}^{A_{IN}{}^{1.5}}\!/\!_{L.A_R}} + 1\right) + 1} \qquad (14)$$

Results and discussion

The three solutions (expressions 8, 11 and 14) differ in the multiplying factor of the term that models the losses due to confinement effects

$$q_G = \frac{q_S}{a.\alpha_B.\beta + 1} \qquad (15)$$

where β is:

β=1/2	C-V flow, case C.
β=1	Full mixed case.

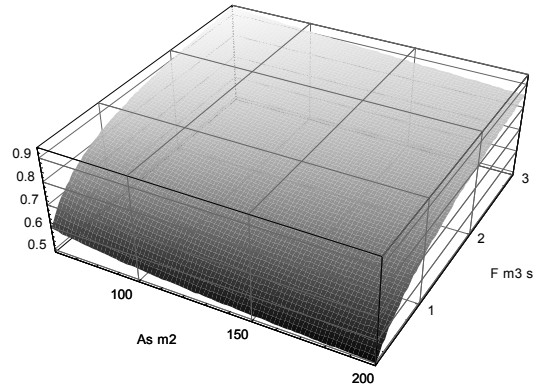

Figure 2.

Plot of expression 14 divided by expression 8. The reduction in heat transfer due to the recirculation can reach 50%. A_{IN}=2m, L=8m.

$$\beta = \left(\frac{1}{0.147}\sqrt{\frac{A_{IN}{}^{3/2}}{L.A_R}} + 1\right) \qquad \text{C-V flow, case R.}$$

in the recirculation case R. The values of β are presented in decreasing order of resultant global heat transfer magnitude (for identical flow rate, surface area, inlet and room surface temperatures). The predictions of the model have been successfully validated using CFD. Figure 2 illustrates the considerable heat transfer reduction that occurs in case R, when compared with the fully mixed case.

Acknowledgements

We would like to acknowledge the financial support of the Fundação para a Ciência e Tecnologia (Lisbon, Portugal) and the California Energy Commission.

References

Awbi H.B., Hatton A.. Mixed convection from heated room surfaces, Energy and Buildings, V.32, (2000) 153-166.

Carrilho da Graca G., Linden P.F.. Simplified modeling of cross-ventilation airflow. Submitted to ASHRAE Transactions, (2002).

Neiswanger L., Johnson G.A., Carey V.P.. An experimental study of high Raleigh number mixed convection in a rectangular enclosure with restricted inlet and outlet openings. Transactions of ASME, V.109, (1987), 446-453.

Siebers D.L., Schwind R.G., Moffat R.J.. Experimental Mixed Convection Heat Transfer From a Large Vertical Surface in a Horizontal Flow. SAND 83-8225, Sandia National Laboratories, Livermore CA, (1983).

Room ventilation and heat transfer in unmixed spaces

Simplified models for implementation in E+

Paul F. Linden[1], Phil Haves[2] , Guilherme Carrilho da Graça[1].

[1]Department of Mechanical & Aerospace Engineering, University of California at San Diego

[2]Commercial Building Systems Group, Lawrence Berkeley National Laboratory

Objectives

- Develop enhanced models to be implemented in E+ to calculate cooling load and air temperatures in unmixed spaces
- Provide implementations of these models in E+

Methodology

- Use dimensional analysis and simplified solutions
- Use experiments in reduced scale water models
- Use CFD simulations to check and refine simple models

The problem of air flowing through a room.

Unmixed flow.

As a result of:

- **Room geometry**
- **Internal heat sources**
- **Inflow momentum flux**

An airflow pattern is established

In order to model ventilation heat transfer it is necessary to determine:

- **The airflow pattern.**
- **Local air temperatures.**
- **Local heat transfer coefficient.**

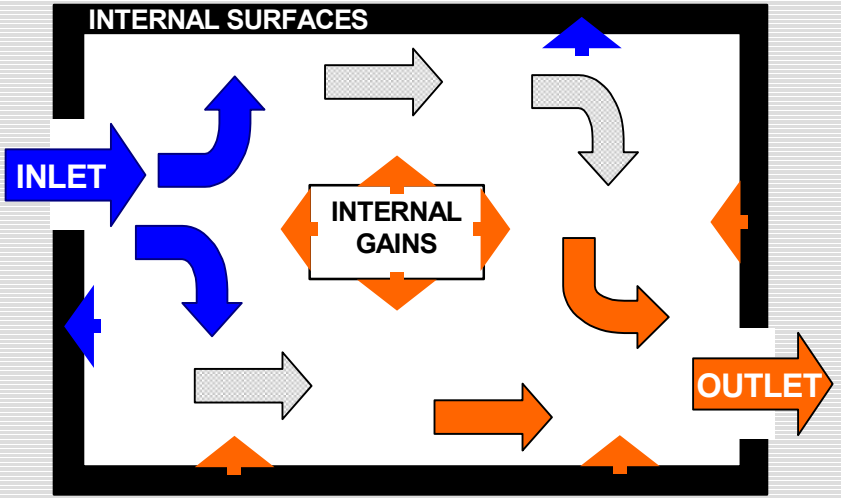

Top View of a room.

Different airflow paths occur with continuous heat exchange with the room surfaces.

Common ventilation strategies

In E+: Mixing ventilation systems are common in most air-conditioned buildings. Absence of a preferred direction for air motion in the room.

Not in E+: In displacement ventilation systems the predominant air movement is vertical, due to heating by internal sources, typically with low momentum fluxes and small horizontal movements across the room

Not in E+: Cross-ventilation occurs when the airflow maintains a significant portion of its inflow momentum as it moves across the room.

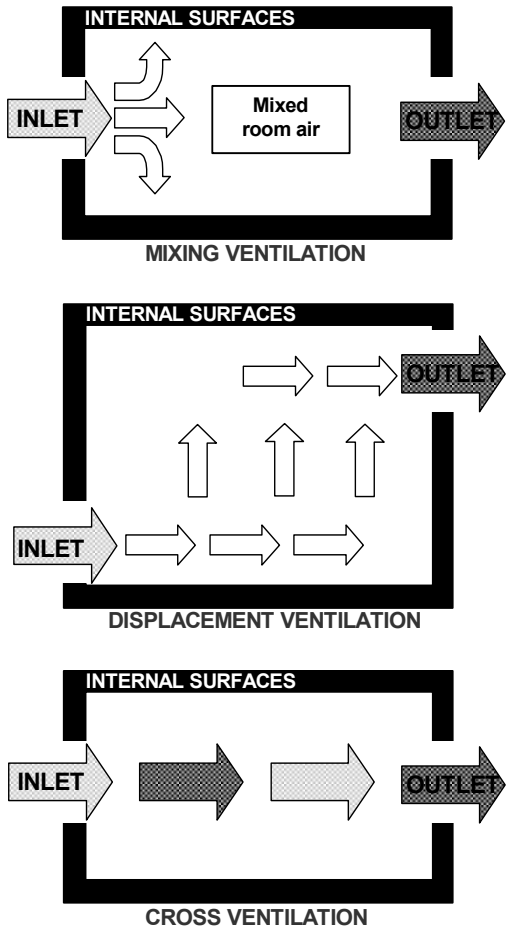

Schematic lateral views of the three commonly used room ventilation strategies.

Implementation of a flow characterization routine.

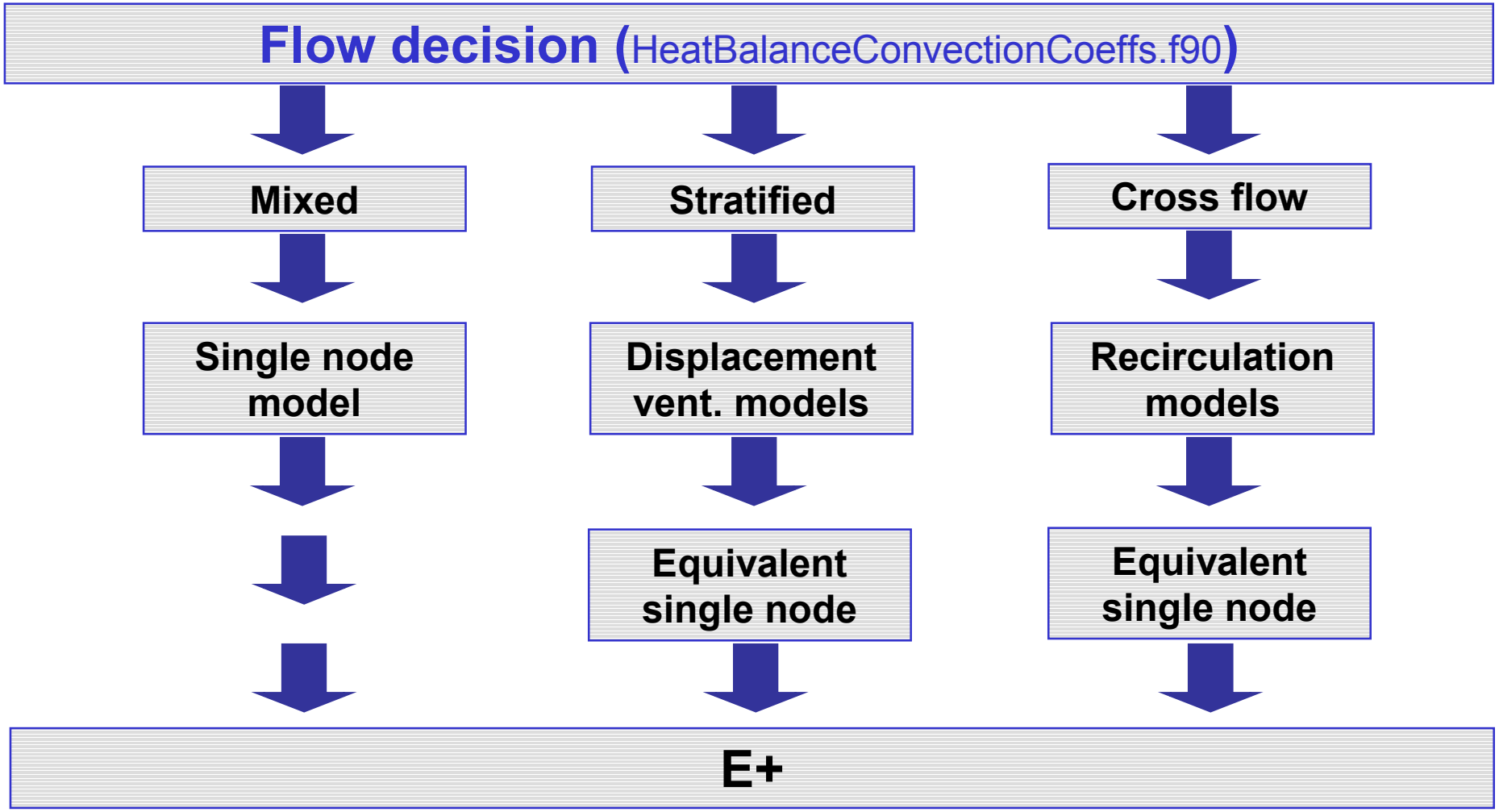

Model operation: displacement ventilation

The model proceeds sequentially through **two steps**:

1-Temperature in the lower half of the room (comfort temperature).

2-Temperature in full mixed upper layer (outlet temp.)

The produces a new **output** (T_D) and requires one new **input** (gp):

Input: gp, fraction of the gains going into the lower layer:

$$gp = \frac{G_D}{G_D + G_U}$$

Output: T_D, temperature in the lower layer, can be used for comfort calculations and thermostat adjustment.

The height of the mixed upper layer is determined in the surface convection algorithm.

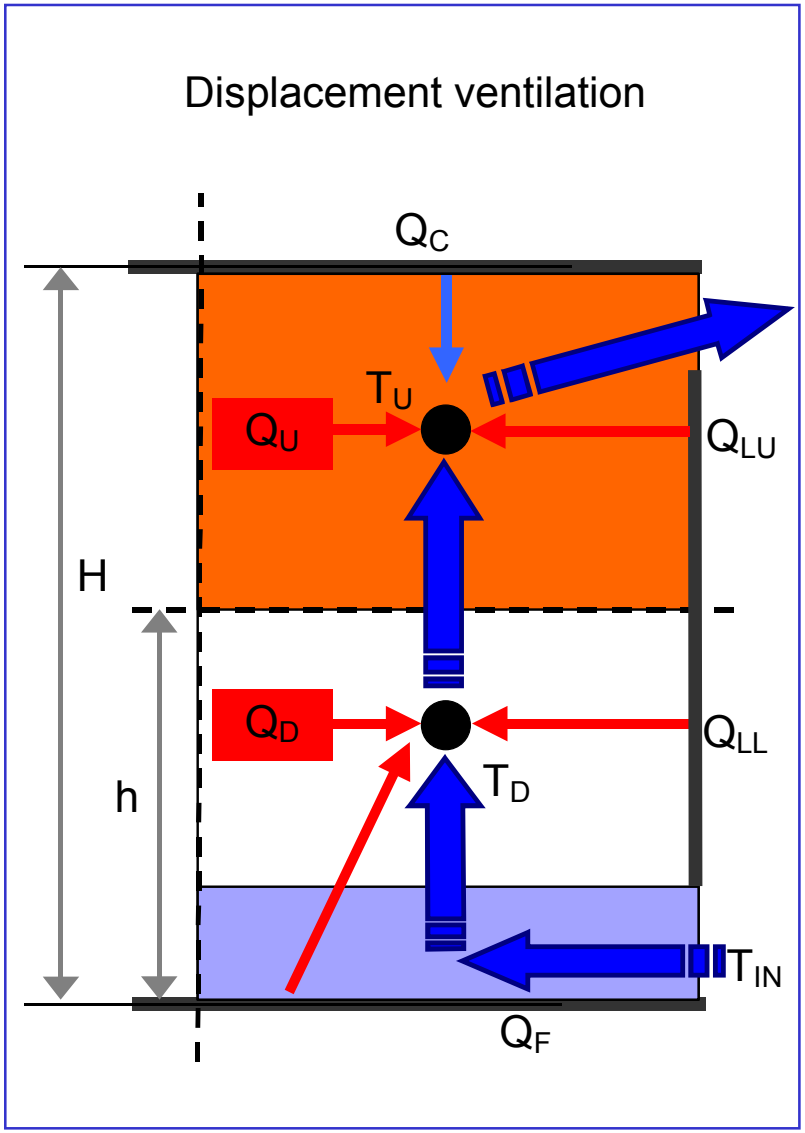

Model implementation using h effective in the DV case

Energy plus uses a single node per room.

The **unmixed ventilation models** can be implemented as a single node using **effective heat transfer coefficients (he)** that adjust to ensure the correct heat flux to the room surfaces.

In the displacement ventilation case **effective coefficients are necessary** for the **lateral** and **floor** surfaces (where contact with the non existent lower would occur).

The **lower node** temperature is given by:

$$Td = -\frac{-G\,gp - HF\,SF\,TF - HL\,hp\,SL\,TL - F\,Tin\,\rho C}{HF\,SF + HL\,hp\,SL + F\,\rho C}$$

And the **effective h for the floor**:

$$HeF = \frac{HF\,(Td - TF)}{-TF - \frac{-G + G\,gp - HC\,SC\,TC - HL\,SL\,TL + HL\,hp\,SL\,TL - F\,Td\,\rho C}{HC\,SC + HL\,SL - HL\,hp\,SL + F\,\rho C}}$$

Mixed model (**E+**)

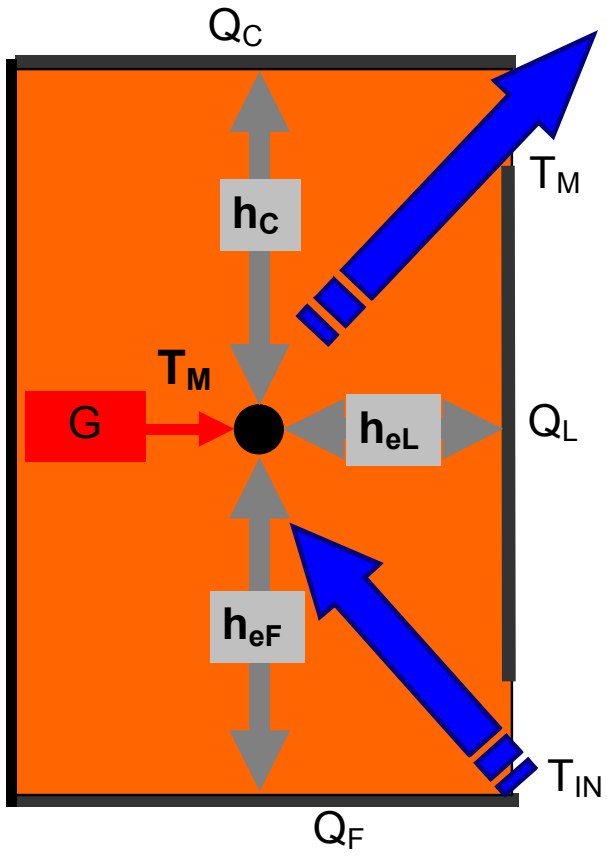

Two layer model: forced and natural flow. Comparison with full mixed model.

Inputs:

G=400W,

H=3m, W=5m,

A_{in},A_{out}=0.5m^2

Surface temp.

Outputs:

Q_C,Q_F,Q_L

T_D, Tout

Flow Rate

Layer height.

Forced Flow

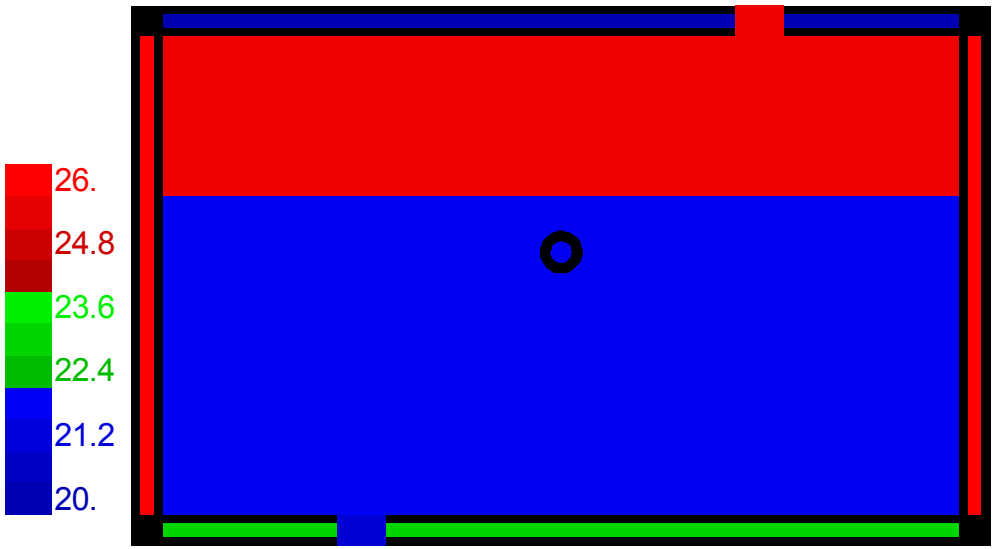

Flow (l/s):	100.
Temp. mixed room:	24.1
Q. mixed room (W):	−29
Q. D.V. room (W):	176
Q. ceiling D.V.(W):	−283
Temp. upper layer:	25.7
Temp. lower layer:	21.7
Temp. inlet:	21.
Temp. ceiling:	20.
Temp. lateral:	26.
Temp. floor:	23.
Upper layer h.(m):	2.

Natural Flow

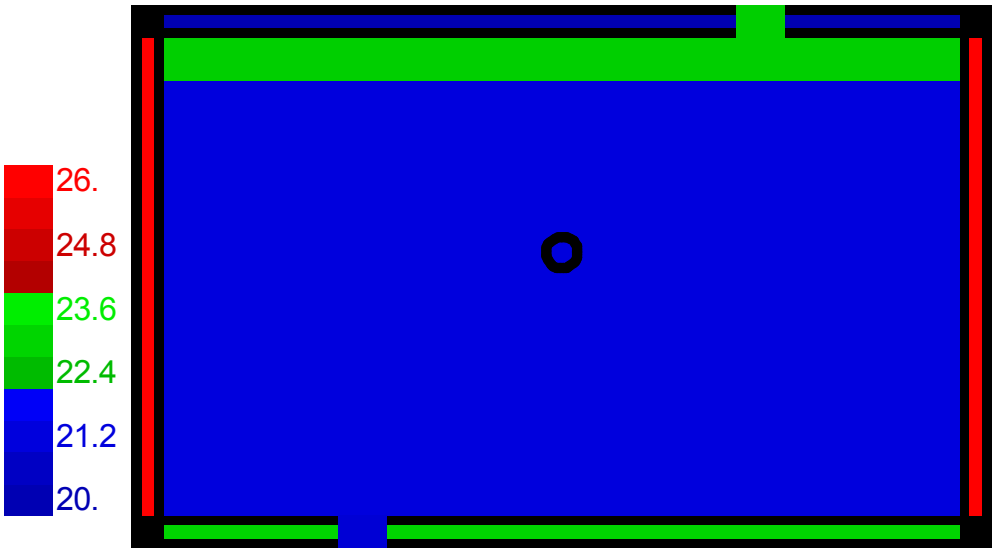

Flow (l/s):	407.9
Temp. mixed room:	22.5
Q. mixed room (W):	324
Q. D.V. room (W):	515
Q. ceiling D.V.(W):	−143
Temp. upper layer:	22.9
Temp. lower layer:	21.2
Temp. inlet:	21.
Temp. ceiling:	20.
Temp. lateral:	26.
Temp. floor:	23.
Upper layer h.(m):	2.7

Two layer model: forced flow, variations with internal heat gains.

The layer height changes.

The full mixed errors are significant.

Large difference in layers and full mixed temperatures

Qp=200W

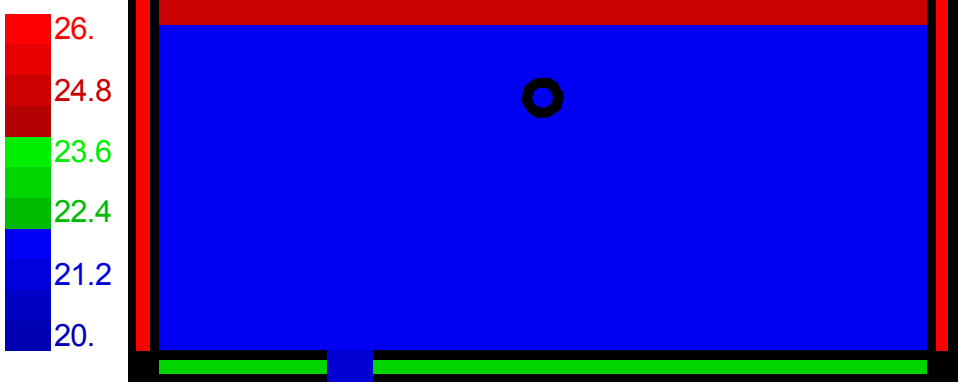

Flow (l/s):	100.
Temp. mixed room:	23.5
Q. mixed room (W):	100
Q. D.V. room (W):	270
Q. ceiling D.V.(W):	−239
Temp. upper layer:	24.8
Temp. lower layer:	21.7
Temp. inlet:	21.
Temp. ceiling:	20.
Temp. lateral:	26.
Temp. floor:	23.
Upper layer h.(m):	2.1

Qp=1200W

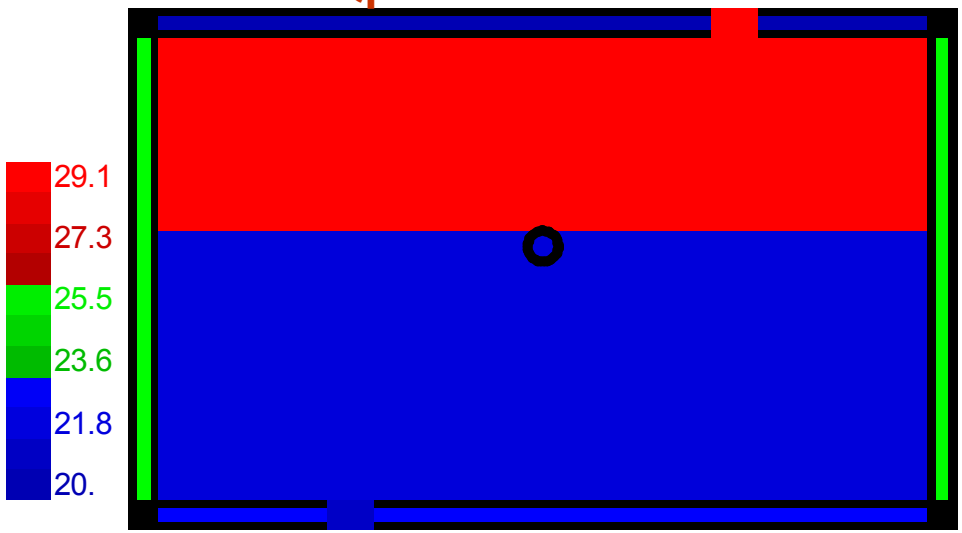

Flow (l/s):	100.
Temp. mixed room:	26.4
Q. mixed room (W):	−547
Q. D.V. room (W):	−211
Q. ceiling D.V.(W):	−455
Temp. upper layer:	29.1
Temp. lower layer:	21.7
Temp. inlet:	21.
Temp. ceiling:	20.
Temp. lateral:	26.
Temp. floor:	23.
Upper layer h.(m):	1.7

Preliminary implementation using h effective in the DV case…

The user chooses the option **HEquiv** for **inside convection algorithm.**

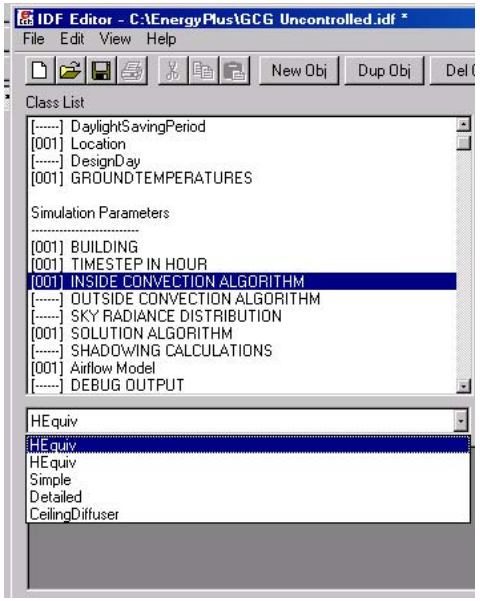

In: HeatBalanceConvectionCoeffs.f90

```
IF (InsideConvectionAlgo == UCSDHEquiv) THEN

G = ZoneIntGain(ZoneNum)%QOECON+ZoneIntGain(ZoneNum)%QOCCON+&
      ZoneIntGain(ZoneNum)%QLTCON+ZoneIntGain(ZoneNum)%QEECON+&
      ZoneIntGain(ZoneNum)%QGECON+ZoneIntGain(ZoneNum)%QHWCON+&
      ZoneIntGain(ZoneNum)%QSECON+ZoneIntGain(ZoneNum)%QBBCON
   TIN=OutDryBulbTemp ! zone air temperature->MAT(ZoneNum)

      TOC= -((-(G*gp) - HF*AF*TF - HL*hp*AL*TLAUX - TIN*MCPI(ZoneNum))/(HF*AF + HL*hp*AL + MCPI(ZoneNum)))


    DO SurfNum = Zone(ZoneNum)%SurfaceFirst,Zone(ZoneNum)%SurfaceLast


      IF (Surface(SurfNum)%Class .eq. 'FLOOR') THEN

        DHF = (-TF - (-G + G*gp - HC*AC*TC - HL*AL*TLAUX + HL*hp*AL*TLAUX - MCPI(ZoneNum)*TOC)/ &
                  (HC*AC + HL*AL - HL*hp*AL +MCPI(ZoneNum)))

        HConvIn(SurfNum) = (HF*(TOC- TF))/SIGN(MAX(ABS(DHF),1.0),DHF)


      ELSEIF (Surface(SurfNum)%Class .eq. 'WALL') THEN

        DHL = (-G + G*gp - HC*AC*TC + HC*AC*TLAUX - TOC*MCPI(ZoneNum) + TLAUX*MCPI(ZoneNum))


        HConvIn(SurfNum) = -((HL*(G - G*gp - G*hp + G*gp*hp + HC*AC*TC - HC*hp*AC*TC + HC*hp*AC*TOC + &
                  HL*hp*AL*TOC - HL*AL*TOC*hp**2 - HC*AC*TLAUX - HL*hp*AL*TLAUX + HL*AL*TLAUX*hp**2 + &
                  TOC*MCPI(ZoneNum) - TLAUX*MCPI(ZoneNum))))/ SIGN(MAX(ABS(DHL),1.0),DHL)

      END IF
    END DO
END IF
```

Model implementation using h effective

Using:

Cubic room (5x5x4m).

Fixed surface temperatures: T_W=17C.

Fixed surface heat transfer coefficients (h=3 W/(m^{2}K)).

1m3/s fixed flow rate (100% outside air).

1KW convective internal gains (gf=0.4).

From the .eso file:

```
2,  1, 7, 1, 0,
1,50.00,60.00,Saturday
6,13.00000
42,3.613457
46,3.613457
50,3.613457
54,3.613457
58,4.022429
62,3.000000
103,14.66341
```

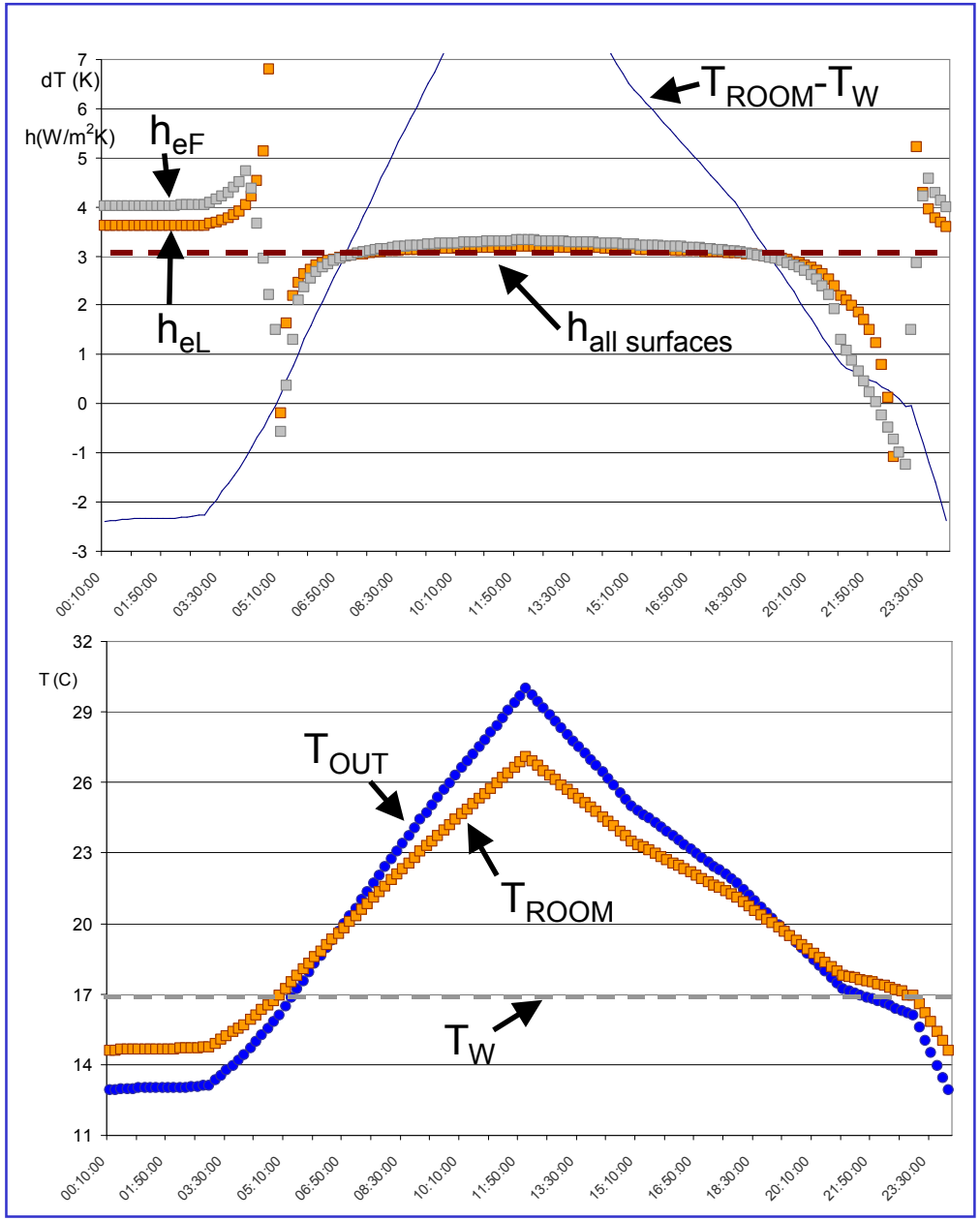

Summary of the DV preliminary implementation

- Requires input of the load distribution (gf)
- Outputs an additional room temperature (Td)
- Operates within the existing E+ one node structure.

- **Next steps:**
- Effects of chilled ceilings etc will be incorporated.
- Breakdown of stratification needs to be characterized.
- Stratification profile and effective buoyancy need to be modeled.

Simplified model for cross ventilation heat transfer

- Allows for **variations of temperature** within the room (**two zones**).
- Includes heat transfer from surfaces taking into **account the flow pattern**.
- Model based on dimensional analysis supported with CFD calculations.
- Room temperatures and overall heat transfer coefficient are a consequence of room geometry and a factor to account for the flow pattern.
- Room **confinement effects** due to the flow **recirculations** are modeled.

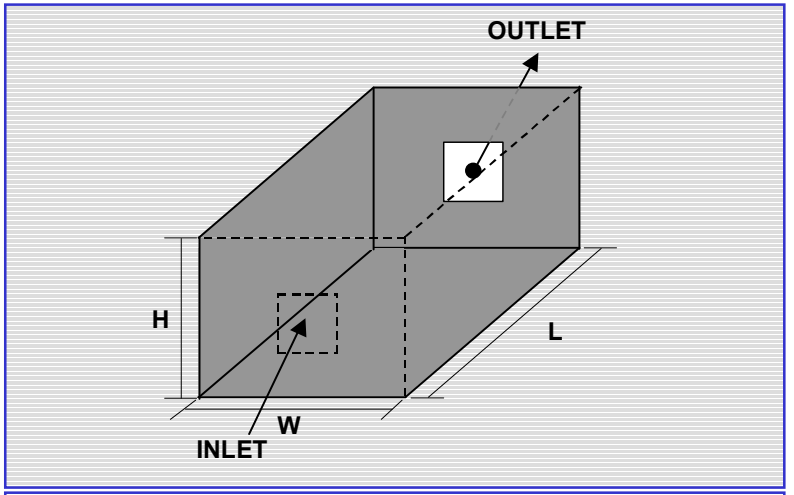

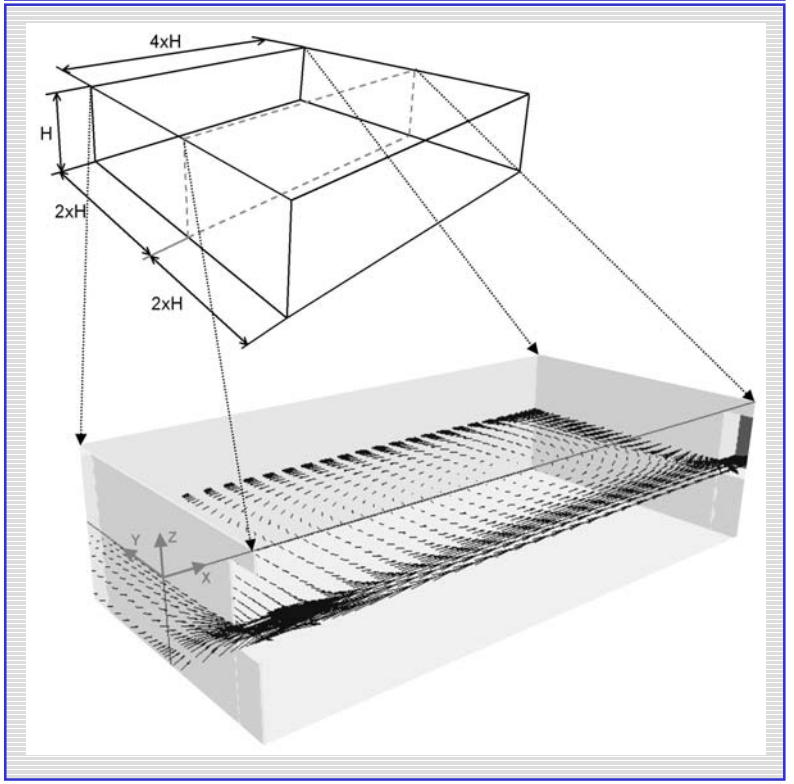

Three possible flow patterns in cross ventilation

The type of flow pattern is determined by:

$$C = \frac{A_{IN}}{A_R}$$

Where: A_{IN} is the inlet area and A_R=Width.Height, is the room cross-section area.

C, $A_{IN}/A_R \cong 1$: the flow attaches to the room walls and is similar to **turbulent flow in a channel.**

CR, $A_{IN}/A_R \cong 0.5$: a **combination of case C and R**. The flow attaches to part of the room perimeter. In most cases, recirculation flow occupies a significant portion of the room.

R $A_{IN}/A_R << 1$: **the flow has two regions**: the **Jet** region, and **recirculation** region.

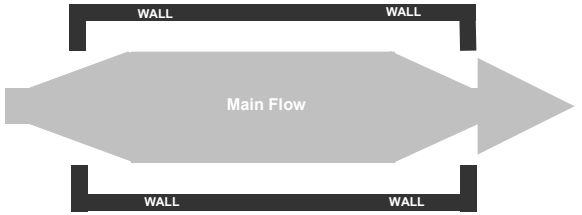

CASE C

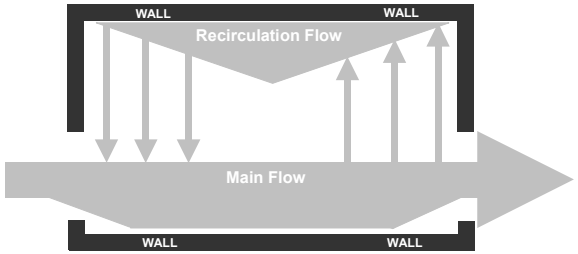

CASE CR

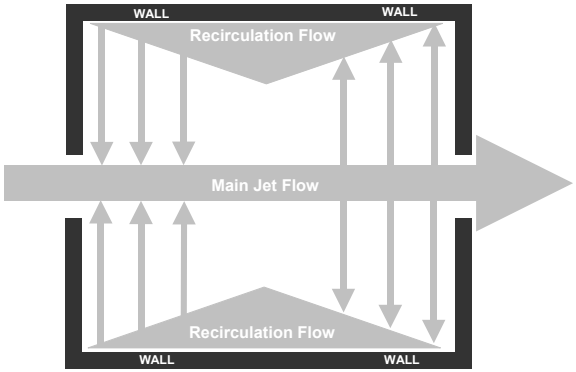

CASE R

Top view of possible flow patterns

Summary of the tasks being performed

- Develop models for:
  - Displacement mechanical ventilation
  - Displacement natural ventilation
  - Cross ventilation
- Produce flow decision maker
- Add enhanced effects such as chilled ceilings

CONTRIBUTIONS TO SIMPLIFIED MODELING OF BUILDING AIRBORNE POLLUTANT REMOVAL

G Carrilho da Graca*, PF Linden

Department of Mechanical and Aerospace Engineering, University of California, San Diego, CA, USA.

ABSTRACT
This paper presents two contributions to simplified modeling of airborne pollutant removal in multi-zone cross-ventilated buildings, applicable on two scales: inter-room flows and in-room pollutant concentration. On the first scale we present an improved cross-ventilation model, obtained by introducing a momentum conservation term in the equation that relates pressure variations to flow through apertures. On the room scale we present an analytical model to predict pollutant levels in two main regions: inlet jet flow and recirculation. The predictions of the model combining these two approaches are compared with CFD simulations of pollutant removal in a multi-zone building. The model retains most of the simplicity of current multi-zone, single node per zone models and can calculate the flow through offset outlet openings, correctly predicting the variation in the flow rates with offset geometry. The predicted airflow and pollutant removal rates display the sensitivity of pollutant concentration to building geometry.

INDEX TERMS
Simple Ventilation Model, Cross-ventilation, Multi Zone Airflow, Computational Fluid Dynamics (CFD), Recirculation.

INTRODUCTION

Currently available simple building airflow and pollutant removal models typically use the Bernoulli equation and a semi-empirical equation that relates pressure variations to flow through apertures (known as the aperture equation) in conjunction with mass and energy conservation principles (Feustel & Dieris, 1991). Several building geometry features and their consequences are modeled: external pressure, internal/external aperture areas and heights, room volume and pollutant sources. Each building zone, or room, is modeled as a fully mixed volume using a single mathematical node.

In their present form, these models can be inaccurate when used to simulate rooms and buildings with multiple outlet configurations, producing both quantitative and qualitative errors. These problems can occur when there is significant conservation of inflow momentum as the air goes through the building, a common flow characteristic in cross-ventilation geometries (Aynsley, 1999). This is due to limitations of the aperture equation, developed mainly for simplified modeling of airflow in ducts with internal restrictions (Idelchik, 1986). These limitations can be shown by comparing aperture equation airflow rate predictions with wind tunnel measurements or numerical solution of the Navier-Stokes equations (Kato *et al*., 1991, Murakami *et al.*, 1992).

* Contact author email: gcg@ ucsd.edu

In addition to this imprecision in multi-zone airflow predictions and resultant pollutant transport, the assumption of a fully mixed room leads to further modeling imprecision by neglecting significant internal gradients that can occur when internal pollutant sources are located in airflow recirculation zones. Recirculations occur whenever the inlet area is smaller than one half of the compartment cross-section area, a frequent geometric configuration (Carrilho da Graca & Linden, 2002).

This paper presents simplified modeling effort that tries to address the two problems described above. With this goal we will present an improved cross-ventilation model, and an analytical model to predict pollutant levels in two main room airflow regions: inlet jet flow and recirculation. The analytical model distinguishes zones in the flow in a similar approach to the common zonal models (Allard, 1992), but does not require iteration or introduce artificial pressure losses between the zones. We restrict attention to horizontal non-stratified flows and passive airborne contaminants or heat, ignoring buoyancy effects.

METHOD

The method used is a combination of simplified solution of the Navier-Stokes equations, experimental correlations and CFD simulations. The theoretical basis of the models will be developed below and limited validation by comparison with a set of cross-ventilation, multi-zone pollutant removal CFD simulations will be presented.

The model is intended to produce first order accuracy and display the system features that dominate the pollutant removal process. In this context, the use of a simple turbulence model in the CFD simulations presented below is considered acceptable, under the verified assumption that the increased numerical load due to the use of a low Reynolds number near wall approach is not needed because the influence of surface boundary layers in multi-zone flow rate prediction is small. The CFD simulations were performed using PHOENICS version 3.3 (PHOENICS, 2000). Figure 1 shows a top view of the system geometries considered in this analysis. The arrows show the possible flow paths in the system. Three square aperture sizes were used, in conjugation with two room sizes. All the apertures were placed at equal distance from the floor and ceiling. The system geometry

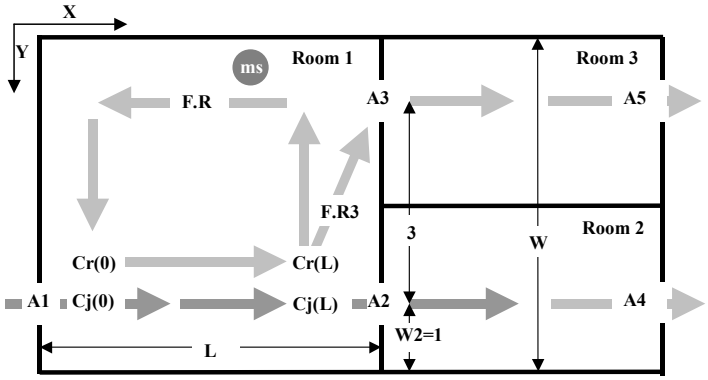

Figure 1. Schematic top view of the geometry of the multi-zone building studied. The building height is equal to 2.25m. In the case with *L*=9m, *W2*=2.5m, approximately $5x10^4$ grid points were used in the simulations. A contaminant source of strength one (ms=1Kg/s), was placed in the recirculation region of room 1, in the region marked ms in the figure. An inflow rate of $1m^3/s$ was imposed in aperture *A1*.

Table 1. Geometric characteristics of the cases analyzed. Length in meters and areas in square meters.

CASE	*L*	*A1*	*A2*	*A3*	*A4*	*A5*
1	6	0.5	1	1	2	2
2	6	0.5	0.5	0.5	2	2
3	9	0.5	0.5	0.5	2	2
4	6	1	1	1	2	2
5	6	1	1	2	2	2
6	6	1	0.5	1	2	2
7	6	1	0.5	2	2	2
8	6	1	0.5	0.5	2	2
9	6	2	2	2	2	2
10	9	2	2	2	2	2

can be scaled with characteristic inlet dimensions (given by the square root of the aperture area). In addition, the flow rates and the pollutant concentrations scale linearly with the inlet flow rate and source strength, respectively. The cases analyzed are shown in table 1.

Figure 2. shows a top view of the CFD airflow and pollutant concentration fields for case 2 (see table 1). The results in this case are representative of the results obtained in all other cases. These figures display the two flow features that we will model: significant momentum conservation, resulting in increased flow rate in room 3 and high pollutant concentration in the recirculation region of room 1, where the source is located.

The corrected aperture equation.

When air flows through an orifice with thin walls there are three main physical processes that lead to energy losses:

1 Flow contraction before the aperture: the trajectory of the fluid particles is altered making them flow towards the axis of the aperture, leading to flow contraction (flow through the aperture actually occurs through a smaller contracted area).
2 Friction losses in the aperture perimeter
3 Shear losses in the expanding jet.

In most buildings, the aperture diameter is much bigger than the wall thickness, and wall shear stresses are negligible in spite of having a fundamental impact on the flow by triggering the turbulent shear layers were most of the dissipation occurs. Further, shear layer losses are much bigger than flow contraction induced losses.

If the flow occupies a large cross section both before and after the aperture, the pressure loss due to the flow through the aperture is given by (Etheridge & Sandberg, 1996):

$$F = C_D A \sqrt{2(P_{IN} - P_{OUT})/\rho} \quad , \tag{1}$$

where F is the airflow rate (m^3/s), A is the aperture area (m^2), P_{IN} is the pressure before the aperture (Pa), P_{OUT} is the pressure after the aperture (Pa), ρ is the density (Kg/m^3). The discharge coefficient C_D is obtained experimentally by measuring the pressure losses for a given flow through the aperture. For thin edged apertures it varies from 0.6 to 0.7. When the flow through the aperture is turbulent, the typical case in building ventilation, the discharge coefficient is independent of the Reynolds number. In the present case, where the flow rate is imposed, the results of the model are independent of C_D.

The aperture equation (1) is used in all the multi-zone flow simulation software tools independently of whether the flow has significant momentum/kinetic energy as it reaches an aperture. This happens whenever air flows unobstructed across a room (after passing through the inlet). The jet flows with constant momentum flux M and with a self similar

profile identical to the inlet (ignoring room confinement effects), so that the kinetic energy flux is given by the product of the maximum amplitude of the jet times the momentum flux. The maximum amplitude of the jet starts to decay like x^{-1} at approximately four jet diameters from the inlet (Malmstrom *et al.*, 1997). The aperture equation can then be corrected by adding a kinetic energy term to the static pressure, obtaining the dynamic pressure. In this case (1) becomes:

$$F = C_D A2 \sqrt{\frac{2}{\rho}\left(\left(P_{IN} + \sqrt[3]{\left(A1/A2\right)^2}\,\rho.V_L{}^2/2\right) - P_{OUT}\right)}\ , \qquad (2)$$

where V_L is the velocity of the flow as it reaches the aperture *A2* (see figure 1). In order to estimate this velocity in the multi-room flow configurations presented below it is necessary to determine if the aperture is in line with flow exiting the previous aperture and also account for the decay in the jet velocity. Clearly, if the model is successful it requires trading improved precision and feedback for increased computational effort and complexity. The factor *A1/A2* in (2) results from imposing kinetic energy conservation. In the calculations presented below, (2) is used to calculate the flow rate through aperture 2, while (1) is used for all other apertures (solutions labeled –CA in figures 3-5). A solution using (1) for all apertures was also implemented, for comparison purposes (label –A in figures 3-5).

Simplified model for pollutant concentration variations in cross-ventilated rooms.
In a fully mixed room model mass conservation leads to the following relation between flow and source strength:

$$F.C = m_S \ \Leftrightarrow C = m_S / F \quad . \qquad (3)$$

Figure 1 shows three locations where the pollutant concentration levels will be calculated in the improved simple model in the recirculation flow when it is re-entrained into the inlet jet flow (Cr(0)), in the inlet jet as it reaches A2 (Cj(L)) and at the beginning of the recirculation (Cr(L), considered equal to the concentration of the air that flows into room 3). The mixing between the jet and recirculation flows is estimated by considering that the interface between these two streams is a self-similar shear layer (Bejan, 1994). It is considered that each stream changes temperature uniformly, a necessary approximation due to the finite volumetric flow rate of both streams. The ratio (R3) between inlet flow rate and flow rate into room 3 is obtained using the corrected aperture equation model. The nondimensional ratio *R* is obtained by subtracting the flow rate R3.F to the recirculation flow rate correlation formula (Carrilho da Graca & Linden, 2002)

$$R = 0.14\sqrt{L.Ar/A1^{3/2}} - R3 \qquad , \qquad (4)$$

where *Ar* is the room cross section area available for recirculation flow (Ar=10m^2). In order to obtain the three concentration values the following system of equations is solved analytically (using σ=12 and $2.\sqrt{A1}$ as an approximation to the mixing perimeter)

$$\frac{\partial Cj(x)}{\partial x} = \frac{V_0.2.\sqrt{A1}}{F.4.\sigma.\sqrt{\pi}}.(Cr(x) - Cj(x)),\ \frac{\partial Cr(x)}{\partial x} = -\frac{V_0.2.\sqrt{A1}}{F.R.4.\sigma.\sqrt{\pi}}.(Cr(x) - Cj(x)) \qquad (5)$$
$$(1-R3).Cj(L) + R3.Cr(L) - ms/F = 0,\ F.(Cr(0) - Cr(L)) - ms/F + r3.Cr(L) = 0$$

RESULTS

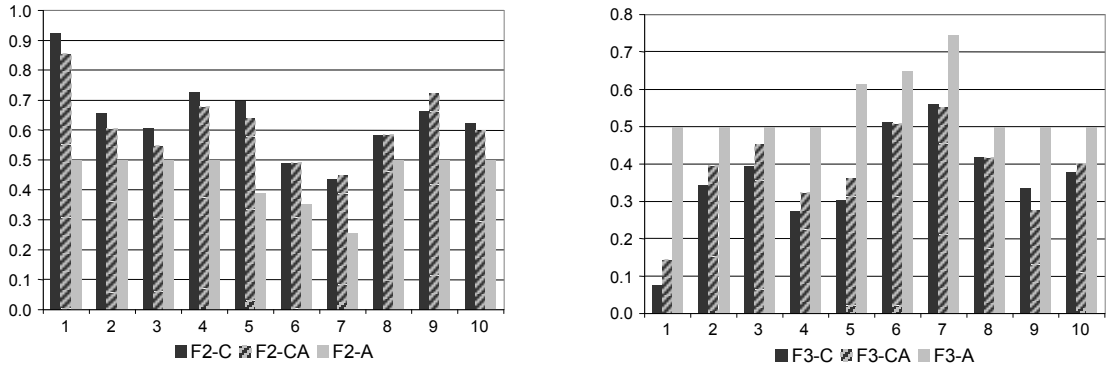

Figure 3. Flow rate though apertures 2 and 3 for the ten cases analyzed. Black: CFD (label C), stripes corrected model (label CA), light gray simple model (label A).

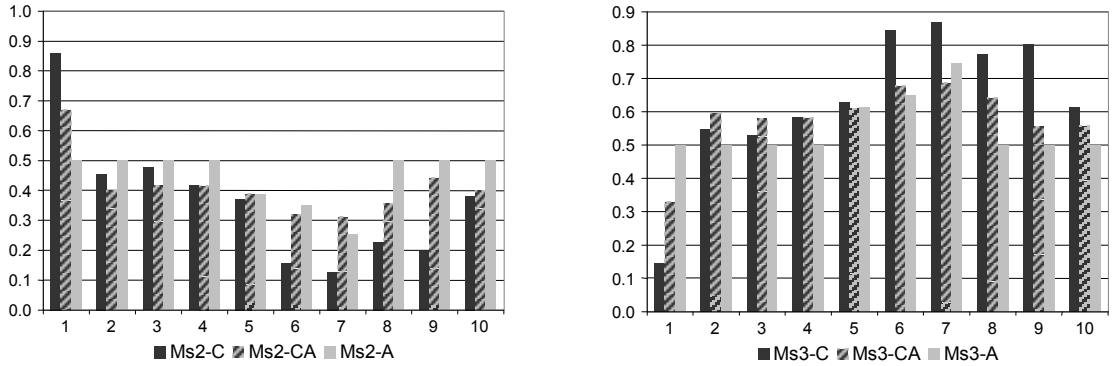

Figure 4. Total contaminant flux, rooms 2 and 3. Ms2=F2.Cj(L), Ms3=F.R3.Cr(L)=F3.Cr(L).

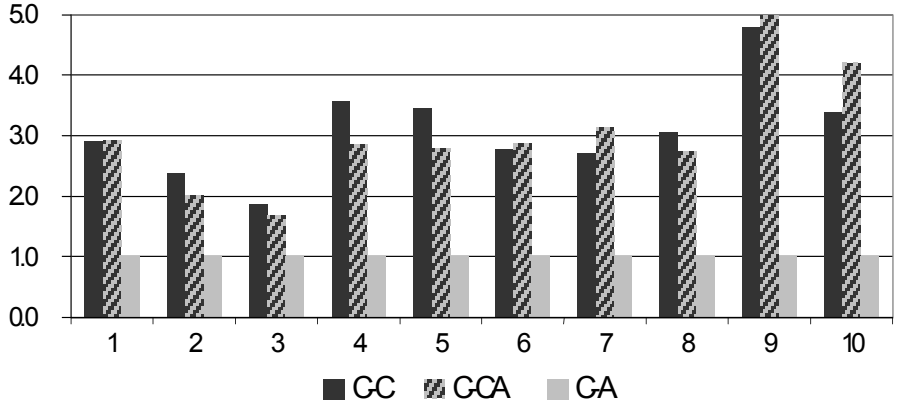

Figure 5. Average concentration in the recirculation region of room 1. Prediction of improved model (-CA) given by: Cr(0). Because the ratio between flow rate and contaminant source is one, existing simple models (label -C) predict a mixed concentration equal to one.

DISCUSSION

The comparison of flow rate predictions presented in figure 3 shows very encouraging results. The results of the corrected model (gray and black) are in close agreement with the CFD-kε simulations, with considerably less computational effort (the most clear example is case 1 in figure 3). As expected, flow rates through room 3 are smaller than through room 2. The model clearly displays the negligible flow rate increase that results from increasing the size of *A3*, on

the flow through *A2* into room 2 (see cases: 4&5 and cases: 6&7 in figure 3). The flow rate predictions presented in figure 3 also represent the contaminant flows into rooms 2 and 3 whenever the dominant contaminant source is the inflow through aperture 1 or a source located in front of the inlet. The predictions of contaminant fluxes when the source is placed in the recirculation region (point "ms" in figure 1) are shown in figure 4. The results are worse than in figure 3, which is due to the fortunate coincidence of higher flow rates and lower concentration that the existing simple model (gray in the figure) predicts for these cases. Even so, the results of the improved model are generally better. Figure 5 shows the value of the average pollutant concentration in the recirculation zone. As expected, the recirculation causes significant pollutant accumulation. The improved model is successful in predicting the effects of variations in room geometry in the concentration levels with first order precision.

CONCLUSION AND IMPLICATIONS

The preliminary validation of this improved simple model indicates that the dominant physical processes in the system are modeled within the first order precision goal.
The improved model retains the simplicity of current multi-zone, single node per zone, models while providing increased feedback on the impact of variations in room and building geometry. The model can be implemented as a refinement on existing simplified software models. In particular, the model calculates the flow through offset openings, and accurately predicts the variation in the flow with offset geometry providing a simple way to estimate pollutant removal efficiency.

ACKNOWLEDGEMENTS

The authors would like to acknowledge the financial support of the Fundação para a Ciência e Tecnologia, Lisbon Portugal and the California Energy Commission.

REFERENCES

Allard F, Inard C. Natural and Mixed Convection in Rooms, Prediction of Thermal stratification and Heat Transfer By Zonal Models, *Proceedings of ISRACVE*, pp. 335-342, Tokyo, 1992. Published by ASHRAE, USA.

Aynsley RM. 1999. Unresolved Issues in Natural Ventilation for Thermal Comfort, Technical Paper, *First International One day Forum on Natural and Hybrid Ventilation*, HybVent Forum'99, Sydney, Australia.

Bejan A. 1994., *Convection Heat Transfer* 2nd ed, Wiley, USA.

Carrilho da Graca G, Linden PF. 2002. Simplified modeling of cross-ventilation airflow. Submitted to: *ASHRAE Transactions*, Technical Paper.

Etheridge D, Sandberg M. 1996. *Building Ventilation: Theory and Measurement*. Wiley.

Feustel HE, Dieris J. 1991. *A survey of air flow models for multizone structures* LBL-30288. Lawrence Berkeley National Laboratory. Springfield, Virginia: National Technical Information Service.

Idelchik IE. 1986. *Handbook of hydraulic resistance*, Hemisphere Pub. Corp., USA.

Kato S, Murakami S, Mochida A, Akabayashi S, Tominaga Y. 1992. Velocity-pressure Field of Cross-ventilation with Open Windows Analyzed by Wind Tunnel and Numerical Simulation. *Journal of Wind Eng. And Ind. Aerodynamics*., 41-44 2575-2586.

Malmstrom TG; Kirkpatrick AT, Christensen B, Knappmiller K. 1997. Centerline velocity decay measurements in low-velocity axisymmetric jets, *J. Fluid Mech*. 346, 363.

Murakami S, Kato S, Akabayashi S, Mizutani K, Kim Y.-D. 1991. Wind Tunnel Test on Velocity-Pressure Field of Cross-Ventilation with Open Windows. *ASHRAE Transactions*: Symposia, USA 525-538.

PHOENICS Version 3.3. 2000. CHAM Ltd., London, UK.

SIMPLIFIED MODELING OF CROSS-VENTILATION AIRFLOW

Guilherme Carrilho da Graça, ASHRAE student member.

Paul F. Linden, ASHRAE member, Ph.D..

ABSTRACT

This paper presents a study of room cross-ventilation airflow. A simplified model is developed using scaling analysis, experimental correlations, and computational fluid dynamics. The model distinguishes two regions in the room, the main jet region and the recirculations, and models relevant flow features that are essential inputs when predicting heat and pollutant transfers as well as indoor thermal comfort conditions. The results of the model are a set of formulas that predict the airflow rates and characteristic velocities in the jet and recirculation flow regions. The formulas clearly display the first order effects of room geometry on cross ventilation airflow characteristics. Simple examples of application of the model to C-V design are presented.

KEYWORDS

air flow, human comfort, indoor air quality, industrial ventilation, jet, passive, simulation, ventilation.

SIMPLIFIED MODELING OF CROSS-VENTILATION AIRFLOW

ABSTRACT

This paper presents a study of room cross-ventilation airflow. A simplified model is developed using scaling analysis, experimental correlations, and computational fluid dynamics. The model distinguishes two regions in the room, the main jet region and the recirculations, and models relevant flow features that are essential inputs when predicting heat and pollutant transfers as well as indoor thermal comfort conditions. The results of the model are a set of formulas that predict the airflow rates and characteristic velocities in the jet and recirculation flow regions. The formulas clearly display the first order effects of room geometry on cross ventilation airflow characteristics. Simple examples of application of the model to C-V design are presented.

INTRODUCTION

Buildings are often designed using energy-inefficient indoor climate control systems. This approach is made possible through intensive use of HVAC equipment. To mitigate these problems, naturally driven cooling systems can be employed. In these cases, air movement through the building is driven by buoyancy forces, or the wind, or a combination of the two.

Modern building systems performance standards create a need for accurate and flexible simulation models. Developing improved models is critical to increased use of low energy or naturally driven cooling. In these systems, the cooling power is variable and often small, making performance simulation and consequent design decisions more challenging and critical to overall success.

The three most commonly used room ventilation strategies are: mixing ventilation, displacement and cross-ventilation (C-V). Mixing ventilation systems are used in most air-conditioned buildings, where cool inflow air introduced through vents near the ceiling mixes with room air, and the resultant momentum diffusion leads to the absence of a preferred direction for air motion in the room. In displacement ventilation systems, the predominant air movement is vertical, due to buoyancy production by internal heat sources, typically with low momentum fluxes and small horizontal movements across the room. Both of these ventilation flows are in contrast with C-V, where significant conservation of inflow momentum occurs with the inlet airflow traveling freely across the room. Poorly designed mixing ventilation systems can exhibit C-V characteristics, with undesirable short-circuiting between inlet

and outlet. ASHRAE (2001) classifies this type of flows as entrainment flow. Cross-ventilated rooms with recirculation regions fit the ASHRAE definition of entrainment flow and can exhibit the characteristic poor mixing between different zones in the room.

Because of the high momentum conservation, C-V configurations are often used when there is need for high ventilation airflow rates. Flows that occur in many naturally ventilated buildings belong to this category, with air flowing through windows, open doorways and large internal apertures across rooms and corridors inside the building. This also occurs in many industrial mechanical ventilation systems and hybrid ventilation systems, for both direct heat and pollutant removal and nighttime structural cooling.

Figure 1 shows a schematic plan view of a cross-ventilated room with internal gains and thermally active internal surfaces. In order to model heat and pollutant transfer and to evaluate thermal comfort, two interrelating components of the C-V system must be modeled. These components are: the airflow pattern (light gray arrows in Figure 1), and determining the magnitude of the local transfers of heat and pollutants between the airflow in its different paths, the internal surfaces and the internal sources (dark gray arrows in Figure 1).

Each of the two parts of the problem poses considerable challenge. By definition, any ventilation airflow pattern has an element of direct air movement between inlet and outlet, but, as will be clear below, in some regions of the room, air can move in other directions. In the local heat and pollutant transfer part of this problem, it is clear from conservation principles that all convective and advective transfers from room surfaces and internal sources will, at one point in the ventilation process, be transferred to the airflow. Transfers between airflow and the internal sources depend on the local concentration gradient and transfer coefficient. In particular, when modeling heat transfer, it is relevant to determine how much energy from the internal gains is transferred to the internal surfaces, and not exhausted by the ventilation air. Clearly, room ventilation transfer problems are composed of two sub-problems that connect in a more or less complex way depending on the ventilation system and room geometry. The model described in this paper will address the airflow pattern component of the C-V modeling problem.

Existing approaches

In order to predict airflow characteristics in C-V, there are currently three available options: computational fluid dynamics (CFD, typically using Reynolds averaged turbulence models), zonal models, and experimental correlations.

The use of CFD requires extensive expertise and time. Further, in many design situations, the precision level and amount of information required and provided can be excessive. Often in these cases the building geometry is not fully defined, making simple modeling approaches and results more adequate than complex flow field simulations. Further, in many situations, designers need to analyze multi-room ventilation geometries using weather data spanning several days or months. In these cases, the use of CFD is impractical and simpler ventilation models are more adequate.

Zonal models simulate indoor airflow by solving for mass and momentum conservation in a set of zones (often less than twenty). These models generally require user identification of the dominant room airflow components (jets, boundary layers, plumes, etc.) that are "contained" in particular zones. Because the momentum equation is not solved in the iteration procedure, an artificial flow resistance is imposed between room zones (Allard & Inard 1992). These features make these models imprecise and often complex to use. As shown below, the model presented in this paper does not impose artificial flow resistances and does not require numerical iteration.

Experimental correlations provide a way to model complex ventilation systems such as C-V of rooms (Givoni 1976; Aynsley 1977; Ernst et al. 1991). However, because these correlations are obtained for particular geometries they lack flexibility to handle variable room geometries.

From a fundamental point of view, all of these three approaches fail to provide simple insights into the mechanisms and system parameters that control the C-V airflow pattern. As mentioned above, high precision may not be required for the design of a cross-ventilated room or building. Simplicity and qualitative identification of the most relevant room geometry parameters and their influence in the airflow pattern are more relevant. As a consequence of the complexity of the problem and the simple solution approach that will be used, first order precision is expected and considered acceptable in view of other uncertainties that are common in building ventilation design, such as furniture geometry, building use, and outside weather conditions.

DEFINING THE AIRFLOW PATTERN

The left side of Figure 2 shows a simple room geometry that can lead to C-V, with an inlet window facing an identical outlet on an opposing room surface. To develop a simple model for airflow in this type of room it is necessary to make approximations that will allow for a simple analysis while retaining the ability to model the

dominant characteristics of the problem. Achieving this goal in the present case requires the use of two types of approximations: in the characterization of the physical processes and in the system geometry.

The main approximations in the system geometry are the following.

1. The model is restricted to rectangular rooms with flat surfaces.
2. Air enters the room through one aperture and leaves through an aperture located in the opposing vertical surface (as shown in Figure 2).
3. The effects of furniture are not considered in detail.
4. The effects of variations in outlet geometry are neglected.

With regard to 4, Baturin (1972) shows experimental evidence of the small magnitude of the effects of outlet geometry, confirmed in the CFD simulations presented below. With these approximations, only five parameters are needed to characterize the room geometry: width W, height H, length L, area A_{IN} of the inlet aperture, and position of the inlet aperture (close to the center or close to the perimeter of the inlet surface).

We begin the analysis of the approximations used in the physical processes with a discussion of the flow regime, a fundamental question when defining the flow pattern. C-V airflows can be seen as an interaction between several "flow elements": a jet, flat surface boundary layers and shear layers. All of these "flow elements" have been studied in detail in the past and their basic behavior can be predicted using simple physical models or correlations. It is then necessary to identify these elements in the C-V flow and determine the flow regime in which they occur.

C-V flows tend to be turbulent in most regions of the room. The main system features that contribute to this turbulence dominated flow are.

- large characteristic room dimensions (typical room depths (L) around: 5-15 m), combined with flow velocities close to the inlet aperture that typically vary between 0.2 and 2 m/s;
- the existence of turbulent "flow elements" interacting in a confined space, such as: the shear layers that begin at the edge of the inlet aperture and expand as the air travels towards the outlet, and the boundary layers that occur close to the room surfaces (see Figure 2);
- significant velocities close the room surfaces (0.1-1m/s). These velocities are generally higher than those commonly found in rooms with HVAC systems.

The shear layers that typically occur in room airflow have a small laminar region (smaller than 0.1m (Bejan, 1994)). In horizontal forced convection boundary layers, transition to turbulence occurs within the first one half

meter (for a forced flow free stream velocity of 0.1m/s or higher). Additional sources of turbulence are: jets impinging on room surfaces, flow around furniture, room corners, and most internal heat sources (generation of turbulence through buoyancy induced flow). Between the different flow elements that can occur in C-V, there may be regions of light shear, almost stagnant flow. Because most of the momentum transfer occurs in turbulent regions the flow is dominated by turbulent processes and regions of laminar flow will not be modeled explicitly. However, the presence of these laminar regions is considered implicitly, since, due to the lower momentum transfer that characterizes them, they form boundaries that establish the spatial limits of the main flow regions.

The C-V flows to which the model applies are bounded by a stationary geometry, have fixed airflow rates and are dominated by horizontal momentum flux, as opposed to buoyancy dominated (which typically occurs in displacement ventilation). For ventilation systems with these characteristics, if the flow regime is stable (predominantly turbulent, as discussed above), the flow pattern will be steady, approximately self similar and suitable for the application of scaling analysis principles. As a consequence, all the velocities in the room are expected to scale linearly with the characteristic velocity of the inlet flow:

$$U_R = C_n . F(L, W, H, A_{IN}, ...). U_{IN} \qquad (1)$$

The function F is expected to depend on L, W, H, A_{IN}, and inlet location. The velocity scale U_{IN} of the inlet jet, will be defined by:

$$M = \int_{A_{IN}} \rho . \left(U_{MAX} . f(\vec{r})\right)^2 dA, \quad U_{IN} = \sqrt{M/\rho A_{IN}} \qquad (2)$$

In order to correlate the velocities in different regions of the room the corresponding correlation constants C_n and scaling laws F must be obtained. By multiplying the velocities in (1) by suitable areas, correlations for flow rates can be obtained. The remainder of this section focuses on defining the flow pattern.

The three types of flow pattern

Figure 3 shows a schematic representation of the three basic airflow patterns that can occur in C-V. Any cross-ventilated room will have an airflow pattern that is either similar to one of the two base cases shown in Figure 3 (cases C and R), or a combination of the two with both recirculation and inlet flow attaching to a lateral surface or the ceiling (case CR).

The simplest flow configuration, case C, commonly occurs in corridors and long spaces whose inlet aperture area is similar to the room cross-sectional area. In this case, the flow occupies the full cross section of the room and the transport of pollutants and momentum is unidirectional, similar to turbulent flow in a channel. The flow velocity profile across the channel is approximately flat due to the high degree of mixing that is characteristic of turbulent flows. The average airflow velocity in the cross section can be obtained approximately by dividing the flow rate by the cross sectional area of the space.

A more complicated airflow pattern occurs when the inlet aperture area is an order of magnitude smaller than the cross sectional area of the room A_R=W.H (for the case shown in Figure 2, A_R=4.H^2). In these cases, the main C-V region in the core of the room entrains air from the adjacent regions and forms recirculations that ensure mass conservation, with air moving in the opposite direction to the core jet flow in some regions of the room (see case R and CR in Figure 3). These recirculating flow regions have been observed in many experiments. The most relevant to the present problem are Aynsley (1976), Baturin (1977), Neiswanger et al. (1987), and Ohba et al. (2001). For these room geometries, when the inlet is located close to the center of the inlet surface, most of the contact between ventilation flow and the internal surfaces occurs in the recirculation regions that occupy the majority of the room volume.

A set of CFD simulations (to be described below), based on geometry similar to Figure 2, confirmed the relation between the non-dimensional coefficient

$$A^* = A_R / A_{IN} , \qquad (3)$$

and the flow pattern. Based on this coefficient it is possible to distinguish the three cases presented in Figure 3:

Case C, $A^* \cong 1$: the flow attaches to the room surfaces and is similar to turbulent flow in a channel.

Case R, $A^* >> 1$: the flow can be divided in two regions: the jet region, connecting the inlet and the outlet and the recirculation region, composed of the return flow that occurs along the cross flow perimeter of the room. In the recirculation region, the maximum velocity occurs close to the internal surfaces and the flow is similar to an attached jet (a wall jet).

Case CR, $A^* \cong 2$: a combination of cases R and C. The jet flow attaches to part of the room perimeter as in case C, still, in most cases the recirculation flow occupies the majority of the room volume.

Most rooms have inlets that are almost one order of magnitude smaller than the room cross-section, resulting in a flow pattern closer to case R or CR. Since the characterization of the flow in case C is straightforward, the following analysis will discuss geometries of type R. These geometries present a considerable challenge because in these cases the transport of heat and pollutants is not unidirectional and there is no analytical solution for the room airflow pattern.

Characterization of the flow in the recirculation regions

As a first step, we analyze the CFD generated velocity field in the horizontal plane of a cross-ventilated room, shown in Figure 2. The flow in the recirculation regions is composed by wall "currents" resembling attached jets that form close to the outlet and are re-entrained in the first half of the path of the inflow jet in the room. These wall currents are bounded by a boundary layer in the region adjacent to the internal surfaces, and, as will be shown below, are subject to pressure gradients that are a consequence of the presence of the inflow jet in a confined space. Because there is no analytic solution for the flow field in the room, the need for a correlation arises as a simple solution to account for room confinement and energy dissipation effects. In the process of developing the correlation, the dominant physical processes in this flow will be identified and modeled.

The recirculation regions are a fundamental part of this C-V flow. The flow rate in the recirculation region, determines the capacity of the recirculating flow to absorb and release heat and pollutants without significant concentration variations. Predicting the velocities in main jet and recirculation regions is essential to estimating comfort and meeting particular design goals (such as maximum and minimum indoor velocities). Due to the importance of jets in the airflow pattern, it is useful to review here the most relevant aspects of jet flow for the present problem.

Characterization of the flow in the jet region

The jets that occur in C-V are approximately axisymmetric for most of the propagation path in the room as long as there is no contact with a room surface. Whenever the jet is close to a room surface, attachment occurs and a wall jet is generated. The velocity scale of the jets can be adequately represented by the average inlet velocity ($U_{JET} \approx U_{IN}$, see (2)), and the characteristic diameter is $\approx \sqrt{A_{IN}}$.

Jets always entrain ambient fluid throughout the propagation path leading to a continuous increase of the transported mass flow rate. In the initial part of the propagation path, a jet is essentially a shear layer that develops along the perimeter of the inlet aperture. When the shear layer reaches the center of the jet, so that it occupies it fully, the jet enters the transition stage and a self-similar, Gaussian, velocity profile is formed. This transition stage is initiated between 4 to 8 diameters from the inlet, and ends at around 20 diameters (Tennekes & Lumley 1994; Malmstrom et al. 1997). In the transition stage, the amplitude of the jet starts to decay.

Because most building apertures have diameters of at least one meter, most jets that occur in C-V do not reach the transition stage in the room (this is the case for the jet shown in Figure 2), possibly reaching the beginning of this transition stage for very long rooms. Most common building apertures, such as doors and windows (not preceded by a corridor with the same section as the aperture), result in an inlet flow that has significant radial velocity due to flow convergence just before the inlet. This is distinct from the square, two dimensional inflow velocity profile that is characteristic of experiments with jets. Still, the jets that occur in C-V flows have shear layers developing from the inlet and a nearly square inlet velocity profile (in the vena contracta region that occurs after the inlet). Further, it will become clear below that any effects from non-square velocity profiles that may exist in the flow are considered in the correlation process by using an integral analysis in conjunction with extensive CFD results.

As consequence of mass continuity, jets occurring in C-V always detrain air close to the outlet, a clear display of confinement effects, typically in the last third of its propagation path in the room (shown schematically in figure 3, cases R and CR). Because there is mass rejection (or detrainment), the flow in this region cannot be classified as jet flow. The magnitude of the confinement effects in the flow can be scaled by comparing the characteristic jet diameter with the room dimensions. Typically, room surfaces are less than ten jet diameters away from the core of the jet at any point of its path in the room. As room dimensions tend towards two orders of magnitude bigger than the jet diameter, the jet tends towards free behavior (Hussein et al. 1994). In this case, the momentum flux in the recirculation flow becomes very small.

Figure 4 shows plots of mass and momentum flux variations in the room (both fluxes across the Y-Z plane) for the case plotted in Figure 2. As expected, from mass conservation principles, the mass flow rate in the return flow varies in proportion with the variations in the mass flow rate of the jet. The momentum fluxes show a similar behavior but, in this case, with more complex implications. The recirculation flux is a negative flux of negative momentum (negative X velocity). Therefore, both momentum fluxes are positive and increase simultaneously

resulting in a total momentum flux that has a maximum close to two thirds of the way along the room. The pressure (not plotted) at the mid-plane level varies, as expected, in opposition to the momentum: a minimum occurs close to halfway along the room. When entering the room the jet is accelerated by a negative pressure gradient. Since the recirculation flow occurs in the opposite direction, this same pressure gradient also makes the recirculation flow stop. Air from the recirculation flow is entrained into the jet in a shear layer with a velocity scale U_{IN} (close to the inlet, the velocity of the recirculation flow is negligible). A positive pressure gradient occurs close to the outlet, an effect of the main jet flow reaching the outlet. This pressure gradient is associated with the deflection of part of the main jet, starting the recirculation flow.

This analysis of Figure 4 allows for a clearer picture of the flow behavior in the room. As the inlet jet propagates across the room, momentum is transferred to the room air, creating an entrainment-driven recirculation flow moving in the opposite direction, with a mass flow rate equal to the entrained flow in the main jet. The total momentum flux of the inflow jet is not constant: as the jet entrains, its momentum flux increases showing a similar trend to the momentum flux in the recirculation flow. Although the jet does not conserve its momentum (it is subjected to a significant pressure gradient), it seems that the recirculation inherits, in the mass rejection stage (close to the outlet), the momentum flux that occurs between the jet and the room air in the entrainment process.

We conclude that scaling wall currents in the recirculations with the inlet jet flow is the key to modeling recirculation flow. In particular, we identify the flux of momentum through the inlet aperture as the dominant flow feature and, the driving mechanism for the recirculation flow. This momentum flows into the room in the form of a jet whose characteristic dimension is typically not more than an order of magnitude smaller than the room length, resulting in a jet flow that is never fully developed and strongly confined.

SCALING LAWS FOR C-V AIRFLOW

If the correlation functions that will be developed are successful, it will be possible to obtain simple analytical expressions that characterize room airflow parameters (both in the main jet region and in the recirculation). In order to obtain the scaling relations, without solving the problem explicitly, the following approximations are used:

- Pressure variations inside the room are not considered. Although there is an assumption that pressure gradients scale with inlet momentum flux, the model will not explicitly include the pressure gradients in the correlation scaling.

- Variations in the momentum flux in the C-V direction will not be considered.
- Effects of drag on the indoor surfaces, and consequent energy dissipation are not considered.
- It is considered that the jet never enters the transition stage before the mass rejection region close to the outlet; consequently, the jet can be modeled as a set of shear layers that develop in its perimeter and never intercept in the core of the jet.
- The analysis will only consider movements in the inflow direction. In some cases there are relevant movements in other directions particularly in rooms with offset apertures.
- The maximum room cross sectional area occupied by the recirculation flow is considered to be a constant fraction of the total room cross-section area. The CFD simulation section shows that this fraction is close to one half for a large array of common room geometries. In this way, the cross section area of the recirculation flow is considered to scale with the room cross section.
- We will consider that all maximum values in the recirculation flow occur in the same location in the room, approximately two thirds along the length, at the point where the main jet flow enters the detrainment stage. The maximum values that are relevant to the correlations are: the fractional area occupied by the flow, the average velocity, the momentum flux, and the mass flux.

Existing work on simple scaling of indoor airflows is well summarized in Etheridge & Sandberg (1996). No models exist for scaling recirculation flows. Jackman (1970) presented an experimentally validated scaling law, based on the existence of a direct scaling relation between inflow momentum flux and overall momentum flux in the room (without distinguishing regions in the flow). The scaling law predicts the average velocity inside rooms with small inlets and high ratio between momentum and mass fluxes (unlike the inlets considered in this study, windows and doors, that typically have small momentum to mass flux ratios). The inlet momentum flux scaling assumption proposed by Jackman (1970) forms the basis of one of the two scaling hypotheses that will be tested in this paper.

The inlet momentum flux is the source of the flow in the room and the interface for inflow/room flow interaction is the shear that develops along the perimeter of the inflow jet. For this reason, inlet and shear layer momentum flux are candidate concepts to scale the momentum flux in the recirculation flow and will be tested using CFD simulations. After the momentum flux is scaled, all other relevant C-V scaling laws can be based on the momentum scaling principle used.

The inflow momentum flux based scaling principle relies on the following sequence of assumptions: pressure variations in the room are proportional to the inlet momentum flux, these pressure variations cause the changes in the return momentum flux of the room air in the recirculation regions. The result of this hypothesis is the following scaling relation between inlet and return momentum flux:

$$\Delta p \approx \rho A_R . U_R^{\,2} \;\Rightarrow\; A_R . U_R^{\,2} \approx A_{IN} . U_{IN}^{\,2} \;\Rightarrow\; U_R^{\,2} = C_M \, A_{IN} / A_R \, . U_{IN}^{\,2} \qquad (4)$$

The right side of (4) is the product of a correlation constant, essential to make this simple analysis feasible, and a non-dimensional function that depends on the system geometry parameters that are more influential in this balance of momentum fluxes (see function f in Equation 1, in this case: $f=A_{IN}/A_R$). The scaling function could have been obtained solely from dimensional analysis by composing a non-dimensional multiplying factor using the three independent length scales in this problem:

1. The square root of the inlet area (see Equation 2).
2. The square root of the room cross section A_R.
3. The room length in the C-V direction, L.

A generic scaling function for this problem has the following form:

$$f = \left(\sqrt{A_{IN}}\right)^m . \left(\sqrt{A_R}\right)^n . L^p \qquad (5)$$

When the correlation function f in Equation 4 is cast in this form we obtain: m=2, n=-2 and p=0. There are infinite possible combinations of the variables in the exponent (m, n and p) that ensure the necessary non-dimensionality (m+n+p=0). The shear layer based correlation hypothesis is obtained by using: m=1, n=-2 and p=1, resulting in:

$$U_R^{\,2} = C_M \frac{\sqrt{A_{IN}} . L}{A_R} . U_{IN}^{\,2} \qquad (6)$$

This scaling relation can also be obtained from simplified solution of the Navier Stokes equations, by evaluating the momentum flux through the shear layer that develops in the perimeter of the inflow jet. The difference between 6 and 5 is the replacement of the square root of A_{IN} by the room length L. According to the shear layer based correlation (6) longer rooms generate higher recirculation momentum fluxes (for similar A_{IN} and A_R).

By manipulating Equations 4 and 6 it is possible to obtain derived correlations for velocity and flow rate in the recirculation region. A correlation for evaluating occupant thermal comfort in this region can be obtained by defining an average velocity in the cross section of the room area that is occupied by recirculation flow (this area scales with

A_R). Finally, multiplying the scaling relation for the average return velocity by the room cross sectional area results in a correlation for the average flow rate. Starting from Equation 4 we obtain:

$$U_R = C_U \cdot \sqrt{\frac{A_{IN}}{A_R}} \cdot U_{IN} = C_U \cdot \frac{F_{IN}}{\sqrt{A_R \cdot A_{IN}}} \tag{7}$$

$$F_R \approx U_R \, A_R \Rightarrow F_R = C_F \sqrt{\frac{A_R}{A_{IN}}} \cdot F_{IN} \tag{8}$$

Similarly for the correlation shown in Equation 6:

$$U_R = C_U \sqrt{\frac{A_{IN} \, L}{A_R}} \, U_{IN} = C_U \sqrt{\frac{L}{A_R \cdot A_{IN}^{3/2}}} \, F_{IN} \tag{9}$$

$$F_R \approx U_R \, A_R \Rightarrow F_R = C_F \sqrt{\frac{L \, A_R}{A_{IN}^{3/2}}} \cdot F_{IN} \tag{10}$$

In addition to these correlations, it is also useful to obtain a scaling relation for the average airflow velocity in the volume occupied by the main jet flow. For this correlation, inflow momentum scaling (Equation 4) will be used, an obvious choice given that this flow region is directly in front of the inlet:

$$A_R \cdot U_J^{\,2} \approx A_{IN} \cdot U_{IN}^{\,2} \Rightarrow U_J = C_{UJ} \cdot \frac{F_{IN}}{\sqrt{A_R \cdot A_{IN}}} \tag{11}$$

CFD SIMULATIONS

In order to test the correlations shown in expressions 4, 6-10, and obtain the corresponding correlation constants that minimize the modeling error, a set of simulations in cross-ventilated rooms was performed. One of the main difficulties when using CFD is the choice and application of Reynolds averaged turbulence model (Wilcox 2000). Of the several models available, the kε model is a common choice because in most cases it can be sufficiently accurate and is relatively simple to use. Because the standard kε model is biased towards simplicity and computational efficiency, the region close to the solid boundaries is not solved numerically, as a way of avoiding the fine resolution needed to handle the high gradients that occur in these regions (in k, ε and in the velocity parallel to the solid boundary (Wilcox 2000)).

In flows that are influenced by solid boundaries the use of wall functions can lead to significant errors. In order to avoid this error source, a low Reynolds number near wall approach can be used, extending the numerical solution of the flow to the region close to the internal surfaces, by using a fine grid in the direction of the main flow gradients. The simulations presented here use the standard kε model in the core flow region (away from room surfaces) and the low Reynolds number model proposed by Lam & Bremhost (1982) close to the room surfaces. In a study by Henkes & Hoogendoorn (1989), this model was among the best low Reynolds number turbulence models (LRkε) for predicting velocity and temperature in a natural convection boundary layer.

The simulations were performed using a commercial CFD package (PHOENICS, 2000). Simulations were considered converged when the normalized residuals were smaller than 10^{-3} and the solution field was stable (the values did not change by more than 10^{-7} (relative change) in each iteration and showed no visible fluctuation or changes after hundreds of iterations).

The results files of the simulations were post processed in order to obtain the momentum flux in the recirculation flow and the other flow characteristics that will be correlated below. Results of simulations for different flow rates showed a linear variation of the velocities in the room with inlet velocity, as expected. As mentioned above, recirculation flow is characterized by negative X velocity. In order to define the jet region a slightly different criteria was used to avoid the inclusion of the stagnation region that separates jet and recirculation. The fraction of the room volume occupied by the jet is calculated by adding all the room volumes where the X velocity at the cell center was bigger than one tenth of the average inlet velocity, avoiding the inclusion of the stagnation regions.

Cases simulated

Appropriate variations of the room geometry were used for all the parameters in the correlations. The values used must conform to the restrictions dictated by common applications in building ventilation as well as a set of restrictions imposed by the approximations in the model. The rules used were:

- The average inlet velocity should be lower than 2m/s. This rule typically results in maximum velocities close to 1.5m/s in the core of the room, a common upper limit imposed by comfort concerns in naturally ventilated spaces.
- The lower limit used for the average inlet velocity was 0.33 m/s. This limit results from two physical restrictions. First, for lower velocities, stagnation and other buoyancy induced effects can have significant

interference in the flow, changing the expected flow pattern that is the basis of the model. Second, turbulent dominated conditions must be ensured in order for the correlations to apply. Natural ventilation flows usually meet or exceed this flow speed.

● Height: 2.25-3.40 m, the lower limit is the common minimum height for a room. The upper limit corresponds to a tall room but does not reach the minimum height for a typical atrium. The model is not applicable to an atrium due to expected buoyancy effects that can change the flow pattern.

● Length: 2.25-13.5 m, the lower limit is typical of small rooms. The upper limit ensures that simulated room jets will be in the developing region for most of the path in the room.

● Width: 2.25-9m, the lower limit ensures that the jet does not attach to the lateral surfaces and recirculation occurs in the flow (one on each side of the main jet flow in the symmetric rooms). The upper limit ensures that the return flow has significant velocity.

Four types of inlets/outlets were used (see Table 1), two windows and two doors:

● A window, with dimensions 1x1m, located at one-meter height (labeled: W).

● A wide window, with dimensions 2x1m, located at one meter height (labeled: WW).

● A door, with dimensions 1x2m (labeled: D).

● A wide door, with dimensions 2x2m (labeled: WD).

Even when restricted to room geometries that conform to the limits described in this section, the variations in room dimensions, in conjunction with all possible inlet and outlet geometries, make testing the correlations a very extensive task. In order to make this task more manageable, the cases analyzed were restricted by choosing discrete values for each of the geometric parameters mentioned above. The different geometries and cases used in the simulations are presented in Tables 1-6.

The model presented in this paper only applies when the flow pattern is dominated by forced convection. For typical rooms, this will occur whenever the room height is $\leq 3.5\text{m}$ and the temperature variation between inlet and outlet are smaller than ≈ 2 °C. When strong buoyancy effects are present in the flow the horizontal recirculations can become undefined and have different characteristics. This case is not treated in this paper.

All the room geometries used to develop the correlation have one inlet and one outlet, with the same dimensions, placed in the center of the inlet and outlet surfaces (the door is placed in the center on the horizontal and adjacent to

the floor on the vertical). The horizontal symmetry of all the cases allowed for the simulation of only one half of the flow domain, simplifying the simulations (see Figure 2).

The model may still be applicable to rooms outside these limits as long as all of the following conditions are verified:

- Most of the jet path in the room is in the shear layer region (the jet does not enter the transition region before two thirds of the room length).
- Buoyancy sources, such as vertical heated or cooled room surfaces, do not dominate the flow.
- The flow is turbulent in the jet region and in the boundary layers close to the room surfaces in the recirculation regions.

The cases simulated were labeled using one letter for the aperture type (W, WW, D and WD), and three numbers for the height width and length. The numbers used for the room dimensions are scaled with room height. The number two is used to label the height in the cases with 3.40 m height for simplicity. All cases where simulated using a one cubic meter per second volumetric flow rate. For all the inlets a turbulence dominated airflow pattern can be obtained for flow rates of 0.5 m^3/s and even lower in the case of the standard window and door (see Table 1). It is important to use similar flow rates for all rooms and aperture types in order to allow for straightforward comparisons between the recirculation flows that result from different geometries.

RESULTS AND ANALYSIS

The constants Cc on the right hand side of Equations 4, 6-11 were determined using linear regression. The obtained linear regression lines (that always pass through the origin) are plotted against the post-processed CFD results for the correlated quantities in Figures 5 a and b, showing the maximum of the momentum and mass fluxes in the recirculation regions as a function of the right hand side of Equations 4&8 (Figure 5-a) and 6&10 (Figure 5-b).

The momentum flux in the recirculation occurs through a fraction of the cross section area, with the reminder occupied by the jet flow. Table 3 shows the designations of the 46 cases used to develop the main correlations. In this table, the line labeled A_F shows the fraction of the room cross-section area occupied by the jet in the point of maximum mass flow rate. Although there is noticeable variation in the values, minimum 0.47, maximum 0.71, most values are close to 0.5. We conclude that, within the first order precision goal, the area occupied by the recirculation

flow can be scaled using A_R (any constant multiplying value, such as one half, is unimportant and will be included in C_C). The adequacy of this and all other approximations is tested in the correlations presented.

Qualitative analysis of Figure 5 shows that the shear layer based correlation is more adequate, in addition, the correlation constant R^2 for the shear layer case, is significantly higher than the inlet momentum flux (R^2=0.75 versus R^2=0.44, see Table 6). Clearly for the set of cases used in this study, shear layer principles are more effective than inlet momentum flux scale the momentum flux of the recirculation flow. The gray lines in Figure 5 represent the recirculation mass flow rate correlations (labeled $C_F(10)$ and $C_F(8)$ in Table 6), again, analysis of this Figure confirms the better results from the shear layer based correlations (from expressions 6 and 10).

Tables 4 and 5 show a set of 20 additional cases where the flow has a different balance, although still characterized by two distinct regions. The common characteristic of the 16 cases, shown in table 4, is a large length to width ratio. In these cases, the flow eventually attaches to the lateral surfaces in the region close to the outlet in the last third of the room length. The flow starts with recirculations but towards the outlet becomes similar to case C, where the momentum flux in the room scales with inlet momentum flux. Further, the maxima of the recirculation flow parameters (momentum, mass and velocity) occur in the first half of the room (as opposed to two thirds or further along the room). Due to their combined nature, partially type R, partially type C, these cases have different slopes in the momentum flux correlations (see correlations labeled (*) in table 6). Further, due to the transition between recirculation and attached flow that occurs in these cases, the flow pattern is expected to be particularly sensitive to furniture and buoyancy effects that are always present in real rooms. Table 5 shows 4 cases where the flow balance is also different from the main set of cases shown in Table 3. In these cases the width to length ratio is large, making the recirculation behave differently, with a small momentum flux (due to the small room length) occurring in a relatively large cross section area.

Clearly, it is essential to develop a simple criterion to distinguish standard C-V recirculation cases from these transitional cases. The criteria that most successfully achieves this distinction is:

$$C_L = \frac{2L}{W - W_{IN}}, \quad 1 \le C_L \le 4 \tag{12}$$

The values of C_L are shown in tables 3-5 for each case (lines labeled C_L). Note that C_L is 4, the transition value, corresponding to rooms with a length to width ratio of less than 2 (depending on the width of the inlet). The ratio on the right hand side of Equation 12 scales the growth of the shear layer that develops at the limit of the main jet flow

(proportional to L) with the available room width for shear layer expansion (on the denominator). The use of the width as the length scale for available space for shear layer expansion reflects the low height to width ratio of the rooms used in the CFD simulations, that leads to jet attachment to part of the floor and ceiling surfaces that are directly in front of the aperture, limiting its vertical expansion. In the case of a room with height comparable to the width it is more appropriate to use a scaling principle based on characteristic diameters of the room cross section and inlet aperture areas.

One important fact displayed by (12) is that rooms where the inlet is placed close to one of the lateral surfaces tend to have more space for shear layer growth. This leads to higher recirculation mass flow rates and velocities. When evaluating these rooms using criteria 12, the factor of two in the denominator must be dropped.

It will be shown below that the flow pattern for cases with C_L bigger than 4 can also be correlated with similar principles, although requiring different correlation constants. The cases in table 5 (C_L<1) where not used to develop the main correlations but are reasonably modeled by these correlations. The correlations are expected to be very imprecise for cases with C_L <1/3 and C_L >11.

The lower limit imposed on C_L already indicates that the model should not be applied when the aperture size is much smaller than the room characteristic length, meaning the model should only be used when

$$\sqrt{A_{IN}} > \frac{\sqrt[3]{L.W.H}}{10} \quad . \tag{13}$$

When the system geometry does not conform to this last criteria, the jet can enter the transition stage while inside the room and many of the approximations explained above are not applicable.

Table 6 shows the slopes of the lines that minimize the error for the correlations described above (these slopes are the correlation constants). From the results shown in this table it is possible to conclude that the correlations proposed achieve first order accuracy. Note that only five of the eleven correlations shown in the Table 6 are adopted in the model, they are:

1. Average recirculating flow velocity in the room cross section with maximum flow rate (1/3<C_L<11):

$$U_R = C_U \sqrt{\frac{L}{A_R . A_{IN}^{3/2}}} F_{IN} \quad , \quad C_U = \begin{cases} 0.298 , & 1/3 \le C_L \le 4 \\ 0.162 , & 4 < C_L \le 11 \end{cases} \tag{14}$$

2. Average volumetric velocity in the main jet region (1/3<C_L<11):

$$U_J = 1.56 \frac{F_{IN}}{\sqrt{A_R . A_{IN}}} \quad , \quad 1/3 \le C_L \le 11 \tag{15}$$

3. Volumetric flow rate of the return flow ($1/3<C_L<11$):

$$F_R = C_F \sqrt{\frac{L\ A_R}{A_{IN}^{3/2}}}.F_{IN} \quad , \quad C_F = \begin{cases} 0.147\ , \ 1/3 \le C_L \le 4 \\ 0.077\ , \ 4 < C_L \le 11 \end{cases} \tag{16}$$

Not surprisingly, the best correlation is for the average velocity in the jet region, successfully predicting a set of cases that has a relative variation of 3.6 (Max/Min line in Table 6), with negligible error. It is interesting to see how accurate the simple shear layer based correlation (Equation 6) is when estimating momentum flux in the cases shown in Table 3. This correlation, obtained from Equation (6) (labeled $C_M(6)$ in Table 6), can predict the momentum flux with an average error of 30% for a set of CFD post processed values with a maximum variation of 27.5 in magnitude. It is relevant to note that the relative errors do not depend on the flow rate. Any interval of flow rate values linearly increases the prediction intervals shown in the fourth line of Table 6, making the final results of the model more impressive.

The correlations labeled with a (*) in this table refer to the cases with $C_L > 4$ (long rooms, shown in Table 4). As expected the slopes in these correlations are always smaller than for the standard correlations (cases in Table 3), as a consequence of the higher dissipation that occurs in long rooms.

Applications to C-V design

In addition to the correlation expressions presented above, when designing cross ventilated rooms two additional ratios can be useful: the ratio between maximum velocity in the room and velocity in the main jet region and the ratio between velocity in this region and velocity in the recirculation.

The first ratio is important whenever a designer must limit the maximum air velocity at any point in the room. The maximum velocity always occurs directly in front and close to the inlet, in the vena contrata region. The fractional contraction of the jet (coefficient C_D) is due to the flow through the inlet and can be obtained analytically for a two dimensional flow, with measurements in three-dimensional flows resulting in similar values (Ohba et al., 2001). The maximum velocity and the desired ratio are given by:

$$\begin{aligned} U_M &= \frac{F_{IN}}{A_{IN}\, C_D}\ , C_D = 0.611 \\ \frac{U_J}{U_M} &= 1.56\ C_D \sqrt{\frac{A_{IN}}{A_R}} \quad , \quad 1/3 \le C_L \le 11 \end{aligned} \tag{17}$$

In some situations the maximum room airflow velocity is a limitation on the design and maximizing the second relation in (17) results in a ventilation system with higher velocities in the jet region of the room while remaining below the maximum allowed velocity (expression 17 is always smaller than one, as can be seen Figure 6-a).

The second relevant ratio is between velocities in the jet region and in the recirculation region, given by:

$$\frac{U_R}{U_J} = C_R \sqrt{\frac{L}{A_{IN}^{0.5}}} \quad , \quad C_R = \begin{cases} 0.191, \ 1/3 \le C_L \le 4 \\ 0.104 \ , \ 4 < C_L \le 11 \end{cases} \tag{18}$$

This ratio is always smaller than one and independent of the room cross-section area. Figure 6-b shows plots of expression 18 for variable inlet areas and room lengths. Longer rooms maximize this ratio up to a limiting length since the flow pattern limitations translated in the criteria shown in expressions 12 and 13 must be respected.

Figure 7-a shows the ratio between inlet flow rate and the recirculation flow rate predicted using (16) for cases with C_L<4. It is interesting to note that for rooms with moderate to large volumes and inlets with areas below 2m^2 this ratio is bigger than one and can even reach three. These high recirculation flow rates are achieved with the above mentioned small momentum fluxes, when compared with the inlet flow, because the flow occurs in a large area, approximately one half of the room cross section (see table 3, line: A_F).

Figure 7-b illustrates possible advantages of using the model in conjunction with other models, in this case the Fanger thermal comfort model (ISO, 1993). The impacts of room geometry and flow rate variations on summer cooling, due to increased air movement, are easily quantified. As expected, higher flow rates and smaller inlet areas result in higher velocities and increased thermal comfort.

So far this paper discussed symmetric rooms or rooms with part of the inlet and outlet perimeters adjacent to the same lateral surface. Asymmetric rooms are very common. Limited, exploratory, simulations for a few of the cases shown in Table 3, using asymmetric inlet/outlet configurations, indicate that the model and the correlations presented above are directly applicable to asymmetric rooms (where the inlet does not face the outlet). It should be noted that in these rooms the smaller of the two recirculation regions tends to have a higher velocity and also reach values of C_L bigger than 4 for smaller length to width ratios. In order to correctly apply the correlation principles to these rooms each recirculation zone should be analyzed independently, applying the correlation formulas twice, using different areas and room widths on each side, a more cumbersome procedure. In this context, for design estimation purposes, the authors recommend the use of the standard correlations, keeping in mind that the results will be less precise.

One last geometry element that is present in most rooms is furniture. Large furniture can change the flow pattern and the recirculation flow characteristics. One straightforward approach to including furniture effects is to define an equivalent room cross-section area, obtained by subtracting the characteristic furniture obstruction area from A_R. Still, it is only a first order estimation of the effects that may, or may not, be applicable depending on the room. The authors will attempt to include general effects of furniture in future developments of the model. The present model should not be used for estimating flow characteristics in rooms where multiple large size floor standing furniture elements occupy more than a third of the room volume or when the inflow jet path is obstructed by furniture.

Using this model in a generic ventilation flow requires several steps:

- First the user must make sure that the room has an inlet facing the outlet, a geometry that leads to C-V.
- Second, the flow must be dominated by forced convection, for typical rooms, this will occur whenever the room height is $\leq 3.5\text{m}$ and the temperature variation between inlet and outlet is smaller than ≈ 2 °C.
- Third the criteria shown in equation 13 must be satisfied, insuring significant momentum conservation.
- Fourth, A^* must be calculated, whenever $A^* \leq 2$ recirculations occur and if $1/3 \leq C_L \leq 11$ then expressions 14-18 can be used to obtain the magnitude of the velocities and flow rates in the two main flow regions. Whenever $A^* \cong 1$ the flow resembles flow in a pipe with a single region (main jet) and modeling is straightforward and does not require correlations.

CONCLUSIONS

The C-V model developed in this paper meets the proposed first order precision goal, while retaining simplicity in its form and application. A simple criterion is introduced, expression 13, that assesses the existence of significant momentum conservation, and therefore C-V, in isothermal flows. Two further criteria are introduced, expressions 3 and 12, allowing for straightforward distinction between different types of C-V flows. The correlations shown in expressions 14-18 model several useful flow parameters in a simple way, making design and control of C-V systems a simpler task.

The obtained expressions and criteria clearly display the effects of the most relevant system geometry parameters and provide simple insight into the mechanisms that control the complex C-V airflow. The functional dependences of the flow characteristics on the different room geometry parameters where clearly identified.

Future developments of the model are: simplified modeling of asymmetric rooms and furniture effects as well as extension of the present analysis method to heat and pollutant transfer in cross ventilation airflows.

The present study should allow for improved understanding of C-V flows and contribute to their increased use, which should lead to reductions in building energy consumption and improved control and confidence in the performance of cross-ventilation systems.

NOMENCLATURE

A_F = minimum room cross-section fraction occupied by the recirculation flow.

A_{IN} = inlet area (m^2).

A_R = room cross sectional area (m^2).

A^* = non-dimensional room area ratio.

C_F = flow rate correlation constant.

C_L = flow scaling non-dimensional criterion.

C_M = momentum correlation constant.

C_n = dimensionless correlation constant (the index n distinguishes different correlated variables).

C_R = correlation constant for the ratio between jet and recirculation velocity.

C_U = velocity correlation constant.

C_{UJ} = correlation constant for the average velocity in the room volume occupied by inlet jet flow.

F = scaling law function.

f = inlet flow profile function.

F_{IN} = inlet flow rate (in m^3/s, given by $U_{IN}.A_{IN}$).

F_R = flow rate in the recirculation region (m^3/s).

M = momentum flux of the jet (in N or J/m).

P = perimeter of the inlet aperture (m).

U_J = average velocity in fraction of the room volume occupied by inlet jet flow (m/s).

U_M = maximum velocity in the room (m/s).

U_R = averaged velocity in a given region of the room that is being modeled (m/s).

W_{IN} = width of the inlet aperture (m).

ACKNOWLEDGEMENTS

The authors would like to acknowledge the financial support of the Fundação para a Ciência e Tecnologia (Lisbon, Portugal) and the California Energy Commission.

REFERENCES

Allard F, Inard C. 1992. Natural and Mixed Convection in Rooms, Prediction of Thermal stratification and Heat Transfer By Zonal Models, Proceedings of ISRACVE, pp. 335-342, Tokyo, 1992. Published by ASHRAE, USA.

ASHRAE. 2001. 2001 ASHRAE handbook-Fundamentals, Chapter 25. Atlanta: American Society of Heating, Refrigeration and Air-Conditioning Engineers, Inc

Aynsley, R.M., Melbourne, W., Vickery B. 1977. Architectural aerodynamics. Applied Science Publisher, London (1977).

Baturin, V. V. , Billington, N. S. 1972. Fundamentals of Industrial Ventilation, Franklin Book Company 1972, pp. 174-179.

Bejan, A. 1994. Convection Heat Transfer 2nd ed, Wiley, USA, 1994.

Ernest D.R., Bauman F.S., Arens E.A. 1991. The Prediction of Indoor Air Motion for Occupant Cooling in Naturally Ventilated Buildings. ASHRAE Transactions 1991, 525-538.

Etheridge, D., Sandberg M. 1996. Building Ventilation: Theory and Measurement. John Wiley & Sons, England, 1996.

Givoni, B. 1976. Man, Climate and Architecture. 2d ed. New York: Van Nostrand Reinhold.

Henks R.A.W.M., Hoogendoorn C.J. 1989. Comparison of turbulence models for the natural convection boundary layer along a heated vertical plate, International Journal of Heat and Mass Transfer 32 (1989), 157-169.

Hussein H.J., Capp S.P., and George W.K. 1994. Velocity measurements in a high-reynolds-number, momentum-conserving, axisymmetric, turbulent jet. Journal of Fluid Mechanics, 258:31, 1994.

ISO. 1993. Moderate Thermal Environments – Determination of the PMV and PPD Indices and Specifications for Thermal Comfort, International Standard 7730, 1993.

Jackman, P. 1970. Air movement in rooms with sill mounted griles – a design procedure. Laboratory report no. 65, Bracknell, UK, 1970.

Lam C.K.G., Bremhost K. 1981. A modified form of the K-ε model for predicting wall turbulence, Transactions of ASME, J. Fluids Eng. 103 (1981), 456-460.

Malmstrom, T.G.; Kirkpatrick, A.T., Christensen, B., Knappmiller, K. 1997. Centerline velocity decay measurements in low-velocity axisymmetric jets, J. Fluid Mech. 346, 363, 1997.

Neiswanger, L., Johnson, G.A., Carey, V.P. 1987. An experimental study of high Raleigh number mixed convection in a rectangular enclosure with restricted inlet and outlet openings. Transactions of ASME, V.109,1987,446-453.

Ohba, M., Irie, K., Kurabuchi, T. 2001. Study on airflow characteristics inside and outside a cross-ventilation model, and ventilation flow rate using wind tunnel experiments. Journal of Wind Engineering and Industrial Aerodynamics, in press, 2001.

PHOENICS Version 3.3. 2000., CHAM Ltd., London, UK, 2000.

Tennekes, H. & Lumley, J.L. 1994. A First Course in Turbulence, Cambridge: The MIT Press, 1994.

Wilcox, DC. 2000. Turbulence modeling for CFD. DCW Industries, La Canada, USA (2000).

Table 1.

Dimensions of the apertures used to develop and test the correlations.

Aperture	Area (A_{IN}, m^2)	Perimeter (P, m)	Average inlet velocity (in m/s, for F_{IN}=1m^3/s)
Window (W)	1	4	1
Door (D)	2	5	0.5
Wide window (WW)	2	6	0.5
Wide door (WD)	4	6	0.25

Table 2.

Dimensions of the rooms used to develop and test the correlations.

Case	21	122	123	221	222	223	141	142	143	144	146	241	242	243	244	246
H (m)	2.25	2.25	2.25	3.5	3.5	3.5	2.25	2.25	2.25	2.25	2.25	3.5	3.5	3.5	3.5	3.5
W (m)	4.5	4.5	4.5	4.5	4.5	4.5	9	9	9	9	9	9	9	9	9	9
L (m)	2.25	4.5	6.75	2.25	4.5	6.75	2.25	4.5	6.75	9	13.5	2.25	4.5	6.75	9	13.5
Vol. (m^3)	23	46	68	35	71	106	46	91	137	182	273	71	142	213	284	425

Ar (m^2) 10 10 10 16 16 16 20 20 20 20 20 32 32 32 32 32

Table 3.

Subset of cases used to develop the main correlations ($1<C_L<4$). A_F is the minimum room cross-section fraction occupied by the recirculation flow.

Case	D122	D123	D142	D143	D144	D146	D222	D223	D242	D243
C_L	2.6	3.9	1.1	1.7	2.3	3.4	2.6	3.9	1.1	1.7
A_F	0.57	0.55	0.54	0.55	0.54	0.53	0.64	0.71	0.53	0.53

Case	D244	D246	W121	W122	W123	W142	W143	W144	W146	W221
C_L	2.3	3.4	1.3	2.6	3.9	1.1	1.7	2.3	3.4	1.3
A_F	0.52	0.53	0.52	0.53	0.56	0.52	0.52	0.52	0.51	0.50

Case	W222	W223	W242	W243	W246	WD122	WD142	WD143	WD144	WD146
C_L	2.6	3.9	1.1	1.7	3.4	3.6	1.3	1.9	2.6	3.9
A_F	0.49	0.50	0.49	0.50	0.49	0.62	0.57	0.55	0.55	0.55

Case	WD246	WW122	WW142	WW143	WW144	WW146	WW242	WW243	WW244	WW246
C_L	3.9	3.6	1.3	1.9	2.6	3.9	1.3	1.9	2.6	3.9
A_F	0.51	0.69	0.55	0.54	0.54	0.53	0.54	0.53	0.52	0.51

Case	W124	W126	W224	W226	WW123	WW124	WW126	WW224	WW226	D124
C_L	5.1	7.7	5.1	7.7	5.4	7.2	10.8	7.2	10.8	5.1
A_F	0.47	0.47	0.48	0.49	0.64	0.62	0.63	0.58	0.57	0.52

Case	D126	D224	D226	WD123	WD124	WD126
C_L	7.7	5.1	7.7	5.4	7.2	10.8
A_F	0.53	0.68	0.63	0.60	0.60	0.60

Table 4.

Subset of cases used to develop the correlations for long rooms (C_L>4).

Case	W124	W126	W224	W226	WW123	WW124	WW126	WW224
C_L	5.1	7.7	5.1	7.7	5.4	7.2	10.8	7.2
A_F	0.47	0.47	0.48	0.49	0.64	0.62	0.63	0.58

Case	WW226	D124	D126	D224	D226	WD123	WD124	WD126
C_L	10.8	5.1	7.7	5.1	7.7	5.4	7.2	10.8
A_F	0.57	0.52	0.53	0.68	0.63	0.60	0.60	0.60

Table 5.

Subset of cases with: 1/3< C_L < 1.

Case	D141	W141	WD141	W241
C_L	0.6	0.6	0.6	0.6
A_F	0.54	0.53	0.55	0.47

Table 6.

Results of the correlations. The corresponding Equation number is shown in parenthesis. The columns signaled with (*) are for C_L>4. All lines pass by the axis origin. The line labeled Max/Min shows the ration between minimum and maximum values obtained from the library of CFD cases used to develop the correlation.

Correlation	C_M(6)	C_M(4)	C_U(9)	C_U(7)	C_U(9)*	C_U(7)*	C_F(10)	C_F(8)	C_F(10)*	C_F(8)*	C_{UJ}(11)
Best Fit Slope	0.032	0.209	0.298	0.680	0.162	0.487	0.147	0.360	0.077	0.231	1.558
Linear Regression R^2	0.75	0.44	0.67	0.42	0.28	0.55	0.88	0.71	0.89	0.83	0.96
Max/Min											

27.5 27.5 4 4 3.7 3.7 10.6 10.6 4.6 4.6 3.6

Average Error (%)

30 60 16 19 19 60 17 28 17 92 5

Maximum Error (%)

111 267 38 72 64 149 55 110 51 163 13

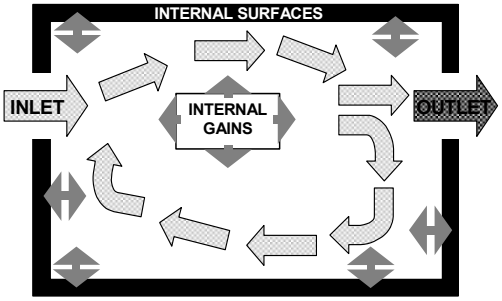

Figure 1.

Schematic plan view of a cross-ventilated room. Dark gray arrows represent heat flow; light gray arrows represent airflow.

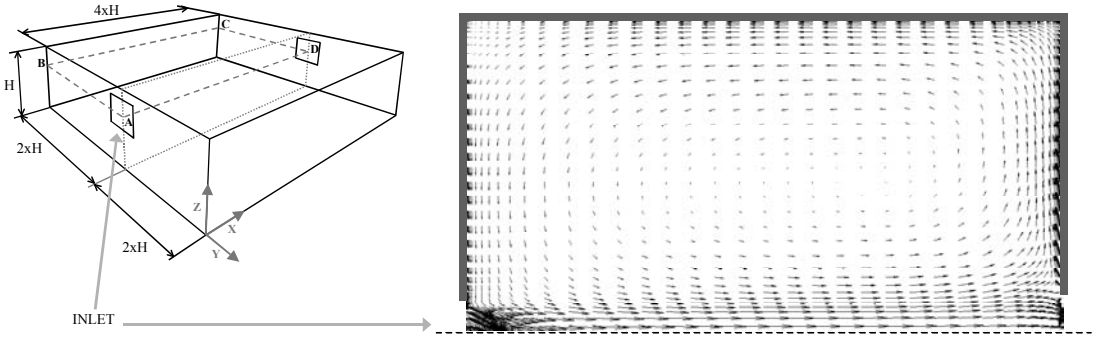

Figure 2.

Left: basic compartment geometry considered in the model (case W144 in Table 3). Right: top view of one half of the velocity field, result of a CFD simulation using the geometry on the left (taking advantage of the system symmetry to simulate only one half of the room volume)

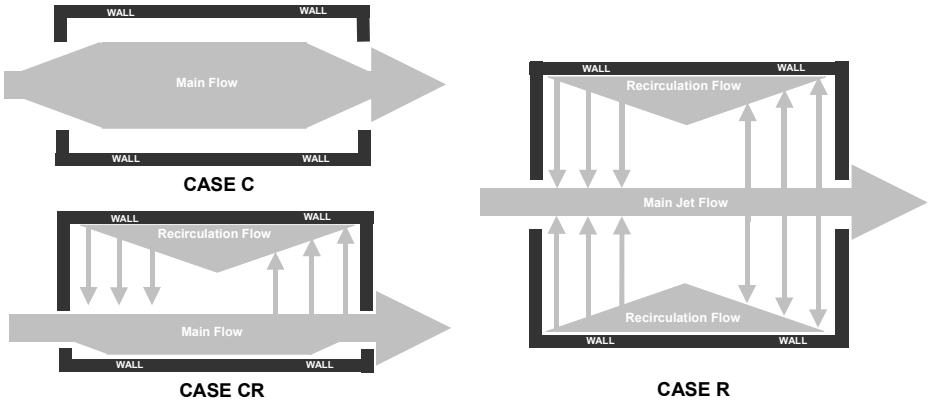

Figure 3.

Top view of the three possible airflow patterns in cross-ventilation.

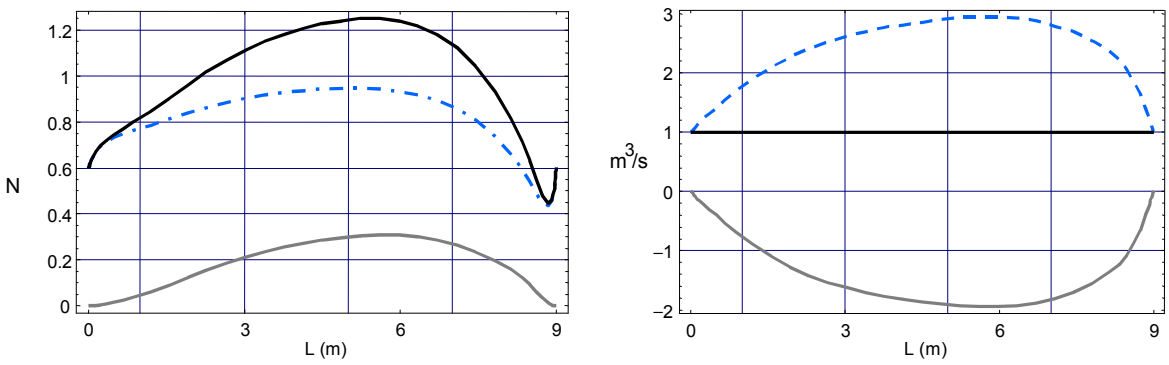

a) b)

Figure 4.

Plots of momentum and mass flux variations for the case plotted in figure 2.
a) Momentum flux in the X direction across the cross section of the cross-ventilation flow (in Newton). b) Mass flux in the X direction in the cross section of the C-V flow (in m^3/s). In both plots: dashed line - total flux in the jet region of the flow - gray line: total flux in the recirculation region, black line - total in the flow.

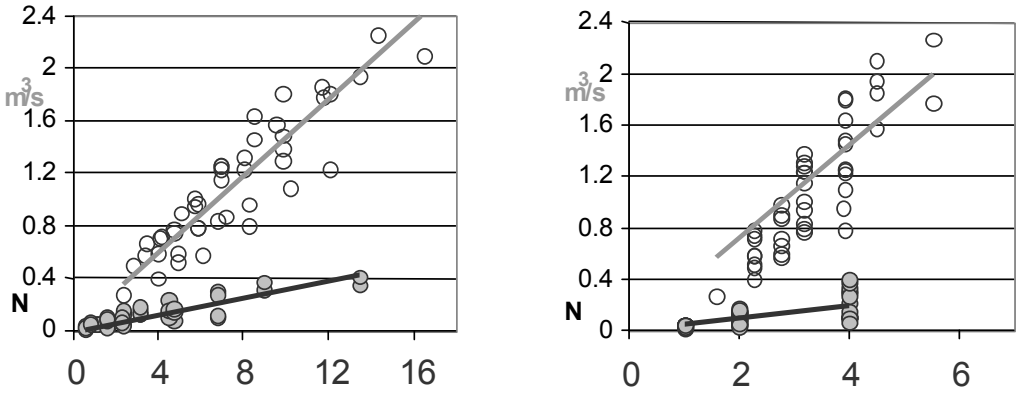

a) b)

Figure 5.

a) correlation lines for shear layer based recirculation momentum flux (black line) and mass flow rate (gray line), b) correlation lines for inlet momentum flux based recirculation momentum flux (black line) and mass flow rate (gray line). In both cases the CFD post-processed results for the cases shown in table 3 (gray dots for the momentum flux and circles for mass flow rate).

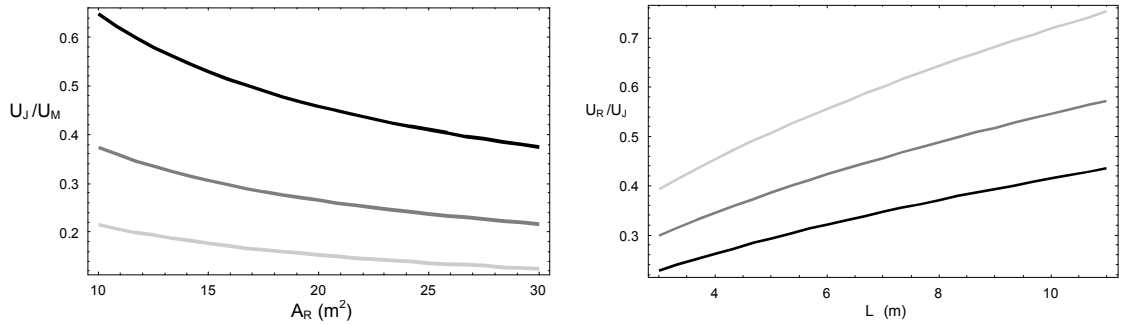

a) b)

Figure 6.

a) Variation with room cross-section area (A_R) of the ratio between the average velocity in the jet region and the maximum velocity in front of the inlet (expression 25). b) Variation with room length (L) of the ratio between the average velocity in the recirculation and in the jet region (expression 26). In both plots, three inlet sizes are used: $0.5m^2$ (light gray), $1.5m^2$ (medium gray) and $4m^2$ (black).

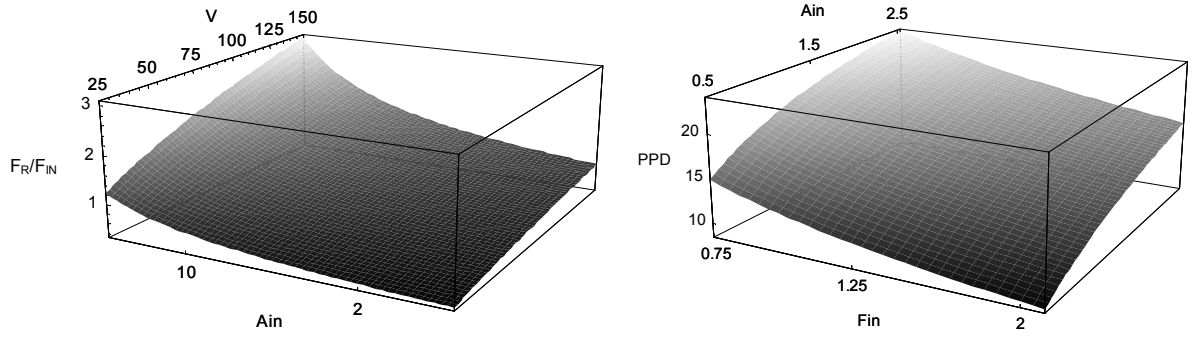

a) b)

Figure 7.

a) Ratio between the recirculation mass flow rate F_{RS} (expression 24) and the inlet volumetric flow rate (F_{IN}), for variable room volume (V in m^3) and inlet aperture area (A_{IN}, in m^2). b) Percentage of people dissatisfied in the recirculation region of a cross-ventilated room for variable volumetric flow rate (F_{IN} (m^3/s)) and inlet aperture area (A_{IN} (m^2)), calculated using Fanger's comfort model (ISO, 1993). Calculation performed using L=8 m, T=27.5 ºC, A_R=15 m^2, a metabolic rate of 1.5 met and standard summer clothing (ASHRAE, 2001).